NAVAL POSTGRADUATE SCHOOL

MONTEREY, CALIFORNIA

THESIS

SIMULATIONS OF DIVERSITY TECHNIQUES FOR URBAN UAV DATA LINKS

by

Poh Seng Cheong Telly

December 2004

Thesis Advisor:	David C. Jenn
Second Reader:	Jeffrey B. Knorr

Approved for public release; distribution is unlimited

THIS PAGE INTENTIONALLY LEFT BLANK

REPORT DOCUMENTATION PAGE	*Form Approved OMB No. 0704-0188*

Public reporting burden for this collection of information is estimated to average 1 hour per response, including the time for reviewing instruction, searching existing data sources, gathering and maintaining the data needed, and completing and reviewing the collection of information. Send comments regarding this burden estimate or any other aspect of this collection of information, including suggestions for reducing this burden, to Washington headquarters Services, Directorate for Information Operations and Reports, 1215 Jefferson Davis Highway, Suite 1204, Arlington, VA 22202-4302, and to the Office of Management and Budget, Paperwork Reduction Project (0704-0188) Washington DC 20503.

1. AGENCY USE ONLY *(Leave blank)*	2. REPORT DATE December 2004	3. REPORT TYPE AND DATES COVERED Master's Thesis	
4. TITLE AND SUBTITLE: Simulations of Diversity Techniques for Urban UAV Data Links			**5. FUNDING NUMBERS**
6. AUTHOR(S) Poh, Seng Cheong Telly			
7. PERFORMING ORGANIZATION NAME(S) AND ADDRESS(ES) Naval Postgraduate School Monterey, CA 93943-5000			**8. PERFORMING ORGANIZATION REPORT NUMBER**
9. SPONSORING /MONITORING AGENCY NAME(S) AND ADDRESS(ES) N/A			**10. SPONSORING/MONITORING AGENCY REPORT NUMBER**
11. SUPPLEMENTARY NOTES The views expressed in this thesis are those of the author and do not reflect the official position of the Department of Defense or the U.S. Government.			
12a. DISTRIBUTION / AVAILABILITY STATEMENT Approved for public release; distribution is unlimited		**12b. DISTRIBUTION CODE** A	

13. ABSTRACT (maximum 200 words)

In urbanized terrain, radiowave propagation is subjected to fading on large-scales and small-scales that would impede on the quality and reliability of data link transmission. This would have implications in many military applications. One example is the performance of unmanned aerial vehicle (UAV) data and communications links in complex urban environments.

The purpose of this research is to study the effectiveness of diversity techniques on the performance of urban UAV data and communications links. The techniques investigated were spatial, polarization, and angle diversities.

The ray tracing software, Urbana Wireless Toolset, was used in the modeling and simulation process. The various combinations of diversity techniques were simulated using a realistic urban city model. For the few transmit-receive geometries examined, it was found that angle diversity with a directive antenna provided the greatest increase in signal strength relative to the no diversity case.

14. SUBJECT TERMS Unmanned Aerial Vehicles, Urban Radiowave Propagation, Spatial Diversity, Polarization Diversity, Angle Diversity, Urbana Wireless Toolset			**15. NUMBER OF PAGES** 115
			16. PRICE CODE
17. SECURITY CLASSIFICATION OF REPORT Unclassified	**18. SECURITY CLASSIFICATION OF THIS PAGE** Unclassified	**19. SECURITY CLASSIFICATION OF ABSTRACT** Unclassified	**20. LIMITATION OF ABSTRACT** UL

NSN 7540-01-280-5500

Standard Form 298 (Rev. 2-89)
Prescribed by ANSI Std. 239-18

THIS PAGE INTENTIONALLY LEFT BLANK

SIMULATIONS OF DIVERSITY TECHNIQUES FOR URBAN UAV DATA LINKS

Poh Seng Cheong Telly
Civilian, Singapore DOD
B.Eng. (Electrical & Electronics), Nanyang Technological University, 2000

Submitted in partial fulfillment of the
requirements for the degree of

MASTER OF SCIENCE IN ELECTRICAL ENGINEERING

from the

NAVAL POSTGRADUATE SCHOOL
December 2004

Author: Poh Seng Cheong Telly

Approved by: Professor David C. Jenn
                 Thesis Advisor

                 Professor Jeffrey B. Knorr
                 Second Reader

                 John P. Powers
                 Chairman, Department of Electrical and Computer Engineering

THIS PAGE INTENTIONALLY LEFT BLANK

ABSTRACT

In urbanized terrain, radiowave propagation is subjected to fading on large-scales and small-scales that would impede on the quality and reliability of data link transmission. This would have implications in many military applications. One example is the performance of unmanned aerial vehicle (UAV) data and communications links in complex urban environments.

The purpose of this research is to study the effectiveness of diversity techniques on the performance of urban UAV data and communications links. The techniques investigated were spatial, polarization, and angle diversities.

The ray tracing software, Urbana Wireless Toolset, was used in the modeling and simulation process. The various combinations of diversity techniques were simulated using a realistic urban city model. For the few transmit-receive geometries examined, it was found that angle diversity with a directive antenna provided the greatest increase in signal strength relative to the no diversity case.

THIS PAGE INTENTIONALLY LEFT BLANK

TABLE OF CONTENTS

LIST OF FIGURES

x

THIS PAGE INTENTIONALLY LEFT BLANK

LIST OF TABLES

THIS PAGE INTENTIONALLY LEFT BLANK

ACKNOWLEDGMENTS

THIS PAGE INTENTIONALLY LEFT BLANK

EXECUTIVE SUMMARY

In military operations in urbanized terrain (MOUT), achieving reliable tactical communications can be challenging. In urban areas, the buildings and structures can result in multipath that leads to fading and excess path loss in radiowave propagation. This problem is evident especially for mobile land forces (i.e., troops and vehicles) that are dispersed at street level confined on two sides by high-rise buildings.

An unmanned aerial vehicle (UAV) with a communications payload can be configured as airborne communications node (ACN) for urban communications capability. A UAV that operates as a communication relay for mobile units operating deep in urban canyons can shorten the communications distance, thus reducing path loss and overcome non-line-of-sight (NLOS) situations. However, multipath and signal fading are still significant.

The ray tracing software, Urbana Wireless Toolkit, from Science Applications International Corporation (SAIC), was used to model and simulate the effects of diversity on urban radiowave links. It is a computational electromagnetic (CEM) tool utilizing a ray tracing engine that combines physical optics, geometric optics, and diffraction physics to produce a 3-D simulation for radiowave propagation.

For urban radiowave propagation modeling, the input parameters for Urbana are CAD facet models for the buildings and roads, including its surface material (e.g. concrete, earth, glass and dielectric properties). The other inputs are the placement, strength, and antenna patterns of transmitters and receivers. The outputs are composite signal strength, angle of arrival and time delay of each arriving signal ray at each receiver or observation point.

In this thesis, three diversity techniques were investigated to assess their performance in an urban environment. They were (1) spatial diversity, (2) polarization diversity, and (3) angle diversity. These techniques were simulated for a UAV platform operating over a small city model. The findings can be summarized as follows. Angle diversity has shown the most significant improvement in received signal strength as compared to the

other two techniques, but the implementation of such directional antennas would be complex. Spatial diversity with two antennas on receive has shown better overall improvement as compared to polarization diversity. Further improvement is possible with more spatially uncorrelated antennas, but its implementation could be limited by the availability of space. Polarization diversity on transmit and receive has shown good received signal strength only in a few cases over the spatial diversity technique. However, a combination of polarization diversity on transmit and spatial diversity on receive has better overall performance. An advantage of polarization diversity is that the two orthogonal linear polarizations can usually be obtained with a single antenna. This is especially appealing for UAV applications, where space on the platform is limited.

This research has demonstrated the potential of implementing diversity techniques for improving UAV data links in MOUT. It should be noted that the simulation performed did not cover all possible system and environment parameters. A limited number of transmitter-receiver geometries were examined. However, care was taken to select cases that included direct line-of-sight (strong signals) and non-line-of-sight in shadows (faded signals). This allows a comparison of various techniques under a range of conditions so that common general conclusions could be reached.

I. INTRODUCTION

A. UAV IN MOUT

Military operations in an urban environment is a tricky business, as history has shown. From Stalingrad (1944) to Somalia (1991) to the current Operation Iraqi Freedom, there are many examples of complex military operations in urbanized terrain (MOUT) where conventional battlefield tactics do not apply. Where urban operations cannot be avoided, some authorities [1] have advocated aerospace operations to be the key for successful MOUT. One increasingly important aspect of aerospace operations is the application of unmanned aerial vehicles (UAV). Figure 1 shows some uses of UAVs for intelligence, surveillance, and reconnaissance operations, and as well for communications relay node.
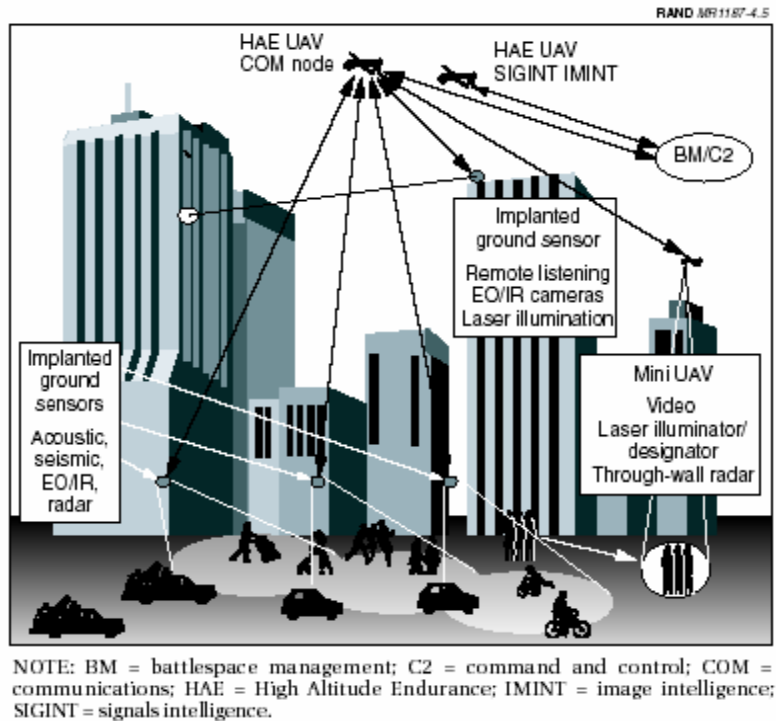
Figure 1.   UAV sensor communications concept (From Ref. [1].)

The suitability of UAVs for MOUT is mainly due to the fact that they can be small and deployed near potential targets with a low probability of detection. They can

1

have long endurance, which is important for surveillance missions that could last for days [2].

In recent years, there is an emergence of mini-UAVs for use in MOUT. Figure 2 shows a vertical take-off and landing (VTOL) Cypher UAV in operation in a confined area. The idea of a small UAV that can be used to provide overhead surveillance, remote sensing, and communications relay would be very useful to troops on the ground.

Figure 2.   VTOL in MOUT (From Ref. [3].)

A mini-UAV can enhance situational awareness by effectively extending the troop's visual range by allowing views around buildings, terrain and other obstacles as shown in Figure 3. Thus, reconnaissance, surveillance and target acquisition can be performed without exposing troops to danger [3]. Similarly, communications effectiveness can be enhanced by using mini-UAVs as relay nodes to reach out to troops in non-line-of-sight (NLOS) situations.
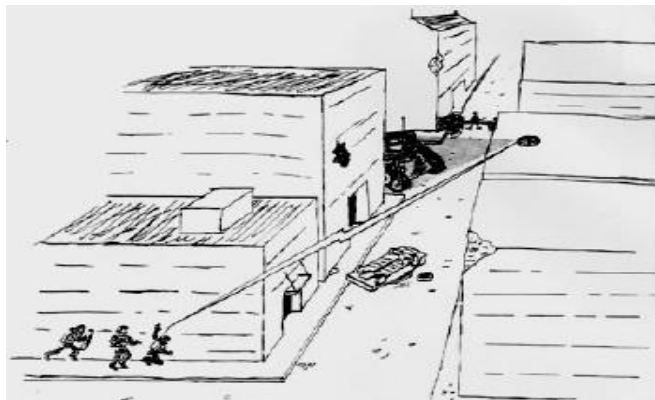
Figure 3.   VTOL providing situational awareness (From Ref. [3].)

Table 1 shows some examples of production mini-UAVs currently on the market. The possible sensors and data link payloads are listed. The data link specifications provide useful information that were adopted in the modeling and simulation performed during the course of this research.

NAME OF UAV	TYPE	MANUFACTURER	SENSORS	DATA LINK
Vigilante 496	Rotary	SAIC	EO/IR, SAR, ESM	900MHz, 2.4GHz
Phoenix	Wing	BAE Systems	IR	J-band
Hermes 450S	Wing	Elbit Systems, Silver Arrow	EO, SAR, Comms relay	C/L-band
Dragon Drone	Wing	BAI Aerosystems	Video/TV	UHF uplink, L-band video with data sideband downlink
Heliot	Rotary	CAC Systemes, Dragon Fly, EDT	CCD, IR	S/Ku-band

Table 1.   Examples of mini-UAVs (Compiled from Ref. [4, 5].)

B.   IMPROVING TACTICAL COMMUNICATIONS IN MOUT

When UAV sensor payloads are used to gather important intelligence and surveillance information, the ability of the UAV to communicate reliably via wireless data links to ground units is crucial. In an urban environment, radio signals can be severely degraded due to multipath and fading, and this can seriously impact the performance of a UAV data link.

Mobile land forces (i.e., troops and vehicles) in MOUT are usually dispersed in so-called urban canyons; that is, at street level confined on two sides by high-rise buildings. Each dispersed unit would need to maintain communications links among each other and with headquarters, for sharing of information to ensure real-time situation awareness. These units are mobile and can be deeply embedded in the urban canyons. As such, it would be difficult to maintain effective communications due to the effects of multipath and fading, excess path loss, and NLOS situations.

In order to alleviate some of the potential communications problems, besides proposing operational limitations, a potential solution is the use of newly evolving technologies including software radios, ultra-wideband waveforms, antenna diversity, and UAV relays [6].

A UAV with a communications payload can be configured as airborne communications node (ACN) for NLOS communications capability between mobile land forces and headquarters [7]. A UAV can reduce the communications link distance and operate as a communication relay for mobile units operating deep in urban canyons. Diversity techniques (frequency, space, polarization, and angle) can be implemented on both the mobile land units and UAV to improve the degraded radio signals which are subjected to multipath and fading.

C.   OBJECTIVES OF THESIS

The purpose of this research is to investigate how to exploit diversity techniques in mitigating the effects of multipath and fading. The focus is to seek improvement on the performance of UAV data links in urban environments. The techniques to be explored are spatial, polarization, and angular diversities.

This research involves modeling, simulation, and analysis of the UAV data link performance. Various spatial, polarization and angular diversity techniques were implemented in simulations in order to study the effects on signal distribution in an urban environment. The modeling and simulation provides insight into the characteristics of urban radiowave propagation and the effectiveness of diversity techniques on the link performance. The mitigating effects on radio signal fading are demonstrated. In summary, this investigation suggests possible methods of improving the performance of UAV data links operating in urban environments.

Parsons [8] highlighted that propagation methods based on the deterministic ray theory have enormous potential. Ray techniques have been used extensively in many investigations in recent years, for both indoor and outdoor environments. Similarly, ray tracing was the primary investigative method for the modeling and simulations of the problems in this thesis. The ray tracing software Urbana from SAIC was used. In addi-

tion, Matlab software was used to assist in the post-processing and visualization of simulation data.

D.   THESIS OUTLINE

Chapter II discusses the characteristics of the urban radiowave propagation channel, and presents some commonly used empirical models.

Chapter III reviews various topics in spatial, polarization and angle diversity techniques, and discusses how they can be used to improve data link performance in an urban environment.

Chapter IV describes the modeling process using the Urbana software and how operation of a UAV data link with diversity can be simulated.

Chapter V describes the simulations and presents data for selected cases.

Chapter VI presents some conclusions and suggestions for further research.

Appendix A lists the Urbana codes used in the modeling and simulations. Appendix B compiles the Matlab codes used in this thesis. Appendix C presents the coordinates system used in Urbana, and Appendix D lists the additional simulations and post-processing results.

THIS PAGE INTENTIONALLY LEFT BLANK

II. CHARACTERIZATION OF URBAN RADIOWAVE PROPAGATION CHANNEL

Urban radiowave propagation is not a single propagation mechanism but a complex combination of direct, reflected, refracted, and diffracted wave components. Depending on the relative strengths and phases of these components, they can interact destructively leading to fading [9].

Propagation between a transmitter and receiver is subjected to three scales of signal fading as shown in Figure 4. They are: (1) large-scale path loss, which refers to the signal variations due to the spreading of wavefront in space over the given environment; (2) shadow fading, which is the signal variation due to the terrain features; and (3) small-scale fading, which are signal variations due to multipath between the transmitter or receiver [10]. In this chapter, these three types of fading are discussed.
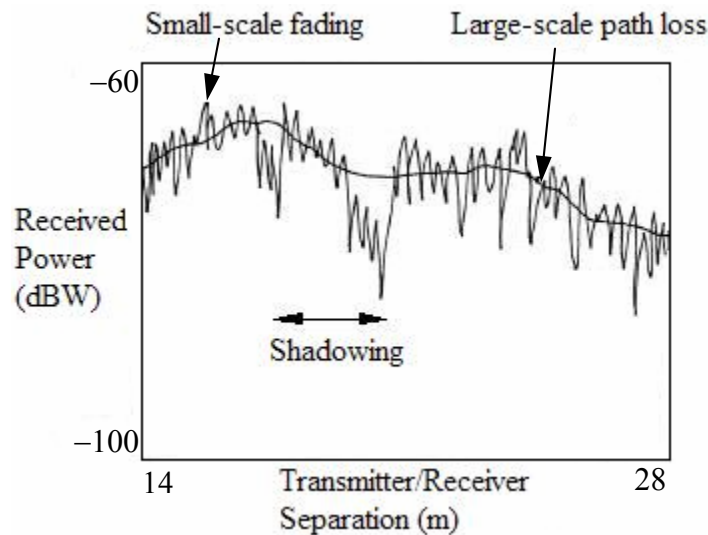
Figure 4.   Received signal in a multipath environment (After Ref. [10].)

A. LARGE-SCALE PATH LOSS MODELS

There are many empirical models that describe the characteristics of large-scale signal loss in an urban environment. However, empirical models are area or city specific, which might not be relevant if the city of interest differs from the reference model. Besides the empirical models, there are deterministic physical models which provide for the

7

flexibility of prediction for specific areas or cities. Ray tracing techniques, which were used in this thesis, are an example. A few of the large-scale path loss models are reviewed in the following paragraphs.

1.   The Okumura–Hata Model

This is an empirical model based on measurements done in Tokyo for frequencies between 200 MHz and 2 GHz. Its urban area is defined as a built-up city or large town with large buildings and houses having two or more stories. For medium to small cities, the total loss is given as [11]

$$L[\text{dB}] = A + B \log R - E \tag{1}$$

where

$$A = 69.55 + 26.16 \log f_c - 13.82 \log h_b, \tag{2}$$

$$B = 44.9 - 6.55 \log h_b, \tag{3}$$

$$E = \left(1.1 \log f_c - 0.7\right) h_m - \left(1.56 \log f_c - 0.8\right), \tag{4}$$

and Equation (4) applies to medium to small cities.

This model is valid for carrier frequencies in the range of 150 MHz $\leq f_c \leq$ 1.5 GHz, transmitter antenna heights in the range of 30 m $\leq h_b \leq$ 200 m, receiver antenna heights in the range of 1 m $\leq h_m \leq$ 10 m, and a transmitter receiver spacing, $R \geq$ 1 km. Under this model, there are other equations for large cities, suburban and open areas, which are not presented here since the city model of interest in this thesis falls into the category of a small city.

2.   The COST 231–Hata Model

In this model, the Okumura–Hata model for medium to small cities is extended to the frequency band 1.5 GHz $\leq f_c \leq$ 2 GHz. The total loss is given as [11]

$$L[\text{dB}] = F + B \log R - E + G \tag{5}$$

where

$$F = 46.3 + 33.9 \log f_c - 13.82 \log h_b \text{ and} \tag{6}$$

$$G = \begin{cases} 0 \text{ dB,} & \text{medium-sized cities and suburban areas} \\ 3 \text{ dB,} & \text{metropolitan areas.} \end{cases} \tag{7}$$

3.   Free Space Loss

In the physical models that are described next, the loss is given relative to the free space path loss, and is referred to as excess loss. The equation for the free space loss is given as [11]

$$L_F = \left(\frac{4\pi r}{\lambda} \right)^2 \tag{8}$$

where r is the distance in meters between the transmitter and receiver antennas and λ the wavelength, also in meters.

With frequency in megaHertz and the distance in kilometers $d[\text{km}]$, the free space loss in decibels is [11]

$$L_F[\text{dB}] = 32.4 + 20 \log d[\text{km}] + 20 \log f_c[\text{MHz}]. \tag{9}$$

4.   The Ikegami Model

In this physical model, diffraction is included and calculated using a single edge approximation at the building nearest to the receiver. The wall reflection loss is given as a constant value. This is shown in Figure 5.
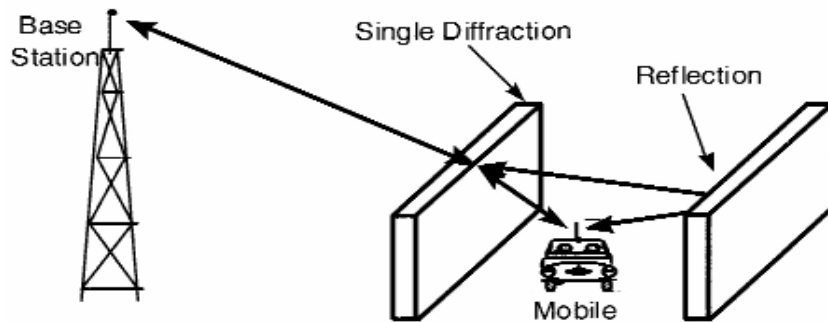
Figure 5.   Physical interpretation of Ikegami model (From Ref. [11].)

9

The path loss equation is given as

$$L[\mathrm{dB}] = L_\mathrm{F} + L_\mathrm{ex} \tag{10}$$

where L_F is the free space loss and L_ex is the excess loss due to the reflection and diffraction.

Based on both reflected and diffracted rays, the equation for the excess loss is given as [11]

$$L_\mathrm{ex}[\mathrm{dB}] = 10\log f_\mathrm{c} + 10\log(\sin\phi) + 20\log(h - h_\mathrm{m})$$
$$-20\log w - 10\log\left(1 + \frac{3}{L_\mathrm{r}^2}\right) - 5.8 \tag{11}$$

where ϕ is the angle between the street and the direct line of sight from transmitter to receiver. The receiver is assumed to be in the middle of the street as shown in Figure 6. In Equation (11), h is the height of the building which causes the diffraction, w is the width of the street (between two buildings) where the receiver is located, and $L_\mathrm{r} = 0.25$ is the fixed reflection loss. This model does not consider the height of the transmitter and the building geometry.
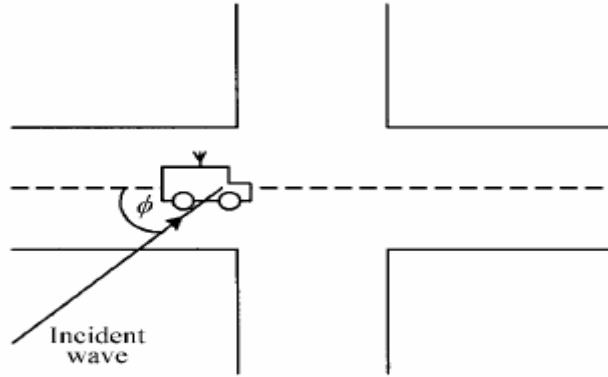
Figure 6.   Physical interpretation of street orientation angle ϕ (From Ref. [8].)

5.   Walfisch–Bertoni Model
In this physical model [8], Walfisch and Bertoni accounted for the transmitter height and building width, which are not considered in the Ikegami model.

From Figure 7, besides the single diffracted and reflected paths (labeled 1 and 2), the total signal at the receiver may have components from multiple rooftop diffractions and reflections (labeled 4) and building penetration (labeled 3). However, these components are assumed negligible [8]. The path loss equation is given as [8]

$$L[\text{dB}] = 32.4 + 20\log f_c[\text{MHz}] + 20\log d[\text{km}] + L_{\text{ex}} \tag{12}$$

where L_{ex} is the excess path loss due to the diffractions and reflections

$$L_{\text{ex}} = 57.1 + A + \log f_c + 18\log d - 18\log(h_b - h)$$
$$-18\log\left[1 - \frac{d^2}{17(h_b - h)}\right] \tag{13}$$

and A accounts for building geometry

$$A = 5\log\left[\left(\frac{b}{2}\right)^2 + (h - h_m)^2\right] - 9\log b + 20\log\left\{\tan^{-1}\left[\frac{2(h - h_m)}{b}\right]\right\}. \tag{14}$$
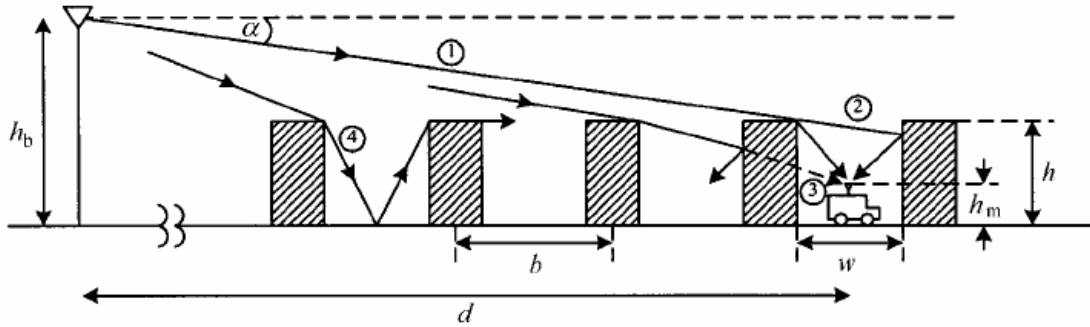
Figure 7.   Physical interpretation of Walfisch–Bertoni model (From Ref. [8].)

6.   COST 231–Walfisch–Ikegami Model

This model gives a better estimation of signal loss in an urban environment because it combines both the Ikegami and Walfisch–Betoni models. The total loss equation is given as [11]

$$L[\text{dB}] = L_F + L_{\text{msd}} + L_{\text{sd}} \tag{15}$$

11

where L_F is the free space path loss, L_{msd} is the multiple-screen diffraction loss due to multiple knife-edge diffraction to the top of the last building, and L_{sd} is for the single diffraction and scattering process down to the street level

$$L_{sd} = -16.9 + 10\log f_c + 10\log\left(\frac{(h - h_m)^2}{w}\right) + L(\phi) \tag{16}$$

where $L(\phi)$ is to account for the street orientation

$$L(\phi) = \begin{cases} -10 + 0.354\phi & \text{for } 0° < \phi < 35° \\ 2.5 + 0.075(\phi - 35°) & \text{for } 35° \leq \phi \leq 55° \\ 4.0 - 0.114(\phi - 55°) & \text{for } 55° \leq \phi \leq 90°. \end{cases} \tag{17}$$

Previously, in the Walfisch–Bertoni model, the transmitter is above the rooftop height. This model extends that model to account for a transmitter height below the rooftop height. The loss equation given as [11]

$$L_{msd} = L_{bsh} + k_a + k_d \log R + k_f \log f_c - 9\log w \tag{18}$$

where

$$L_{bsh} = \begin{cases} -18\log\left[1 + (h_b - h)\right] & \text{for } h_b > h \\ 0 & \text{for } h_b \leq h, \end{cases} \tag{19}$$

$$k_a = \begin{cases} 54 & \text{for } h_b > h \\ 54 - 0.8(h_b - h) & \text{for } R \geq 0.5 \text{ km and } h_b \leq h \\ 54 - 0.8\dfrac{(h_b - h)R}{0.5} & \text{for } R < 0.5 \text{ km and } h_b \leq h, \end{cases} \tag{20}$$

$$k_d = \begin{cases} 18 & \text{for } h_b > h \\ 18 - 15\dfrac{(h_b - h)}{h} & \text{for } h_b \leq h, \end{cases} \tag{21}$$

and

$$k_f = -4 + 0.7\left(\frac{f_c}{925} - 1\right) \text{ for medium-sized city.} \tag{22}$$

12

B.   SHADOW FADING

In an urban environment, there are signal variations due to changes in building heights, widths, shapes, the street width, and the presence of street lamps and trees. The distribution of such fading is log-normal because the signal, when measured in decibels, has a normal distribution. The standard variation of the log-normal distribution for the shadow fading is also known as the location variability, σ_L [11]. In mobile communications the shadow fading variation has found to be in the range of $6 \le \sigma_L \le 12$ dB [12].

C.   SMALL-SCALE FADING

When a transmitter or receiver is surrounded by buildings or structures, they reflect, scatter and diffract the transmitted radiowaves. The result is that several waves arrive at the receiver via different directions and paths. These different radiowaves can result in either signal strength addition or subtraction at the receiver, because the signals have different phases, which are independent and uniformly distributed from 0 to 2π.

The Rayleigh distribution is an excellent representation for the signal strength variations in NLOS situations due to small-scale fading. It is also known as Rayleigh fading [11].

In LOS situations, the received signal consists of the Rayleigh distributed signal plus a LOS signal. The resultant signal strength variations follow a Rician distribution. This Rician distribution applies whenever one signal path is much stronger than the other multipath components [11].

D.   RAY TRACING METHOD

The previous sections have presented the basic propagation mechanisms and phenomena such as large-scale path loss, the effect of shadowing, and finally the statistical characteristics of small-scale fading. These mechanisms contribute to the path loss and power fading of radio signals in an urban environment.

The ability to predict the fading is important when planning a mobile radio system to be deployed in a particular environment or area. The predictions can be included in the

planning and operation of such a radio system to ensure efficient and effective communications coverage over the desired area [8]. Ray tracing, which uses computational numerical methods, is an efficient way of predicting the fading.

Ray tracing uses a deterministic approach. Rays are traced from the transmitter and allowed to interact with the environment yielding diffracted, reflected, and transmitted (partially absorbed in the process), components at a given receiver location. The lengths of the various ray paths give the amplitudes and phases of signal components arriving at the receiver. The strengths of reflected and transmitted rays are computed using geometrical optics (GO), and for diffracted rays, the geometric theory of diffraction (GTD) [13].

1. Geometrical Optics

Geometrical optics uses simple ray tracing to find an approximate field strength at the receiver using plane wave Fresnel reflection and transmission formulas [11]. The total GO field is given as [11]

$$\mathbf{E_{GO}} = \mathbf{E}_0 A_0 e^{-ik_0 r_0} + \sum_{i=1}^{N_i} \mathbf{R}\mathbf{E}_i A_i e^{-ik_i r_i} + \sum_{j=1}^{N_t} \mathbf{T}\mathbf{E}_j A_j e^{-ik_j r_j} \qquad (23)$$

where $\mathbf{E_{GO}}$ is a 2-by-1 column vector with elements corresponding to the horizontal and vertical polarized field components. The other quantities in Equation (23) are:

N_r, N_t, the total numbers of reflected and transmitted traced rays, respectively,

r_n, the distance along n^{th} ray,

k_i, the wavenumber associated with the medium in which the ith ray propagates,

A_i, the spreading factor for the ith ray,

$\mathbf{E}_{i,j}$, the 2-by-1 incident field vector at the corresponding transmission or reflection point,

$\mathbf{R}$, a 2-by-2 reflection coefficient matrix, and

$\mathbf{T}$, a 2-by-2 transmission coefficient matrix.

The spreading factor, $A_i = 1/r_i$, is used for spherical waves and plane boundaries. Figure 8 shows some examples of reflection and transmission.
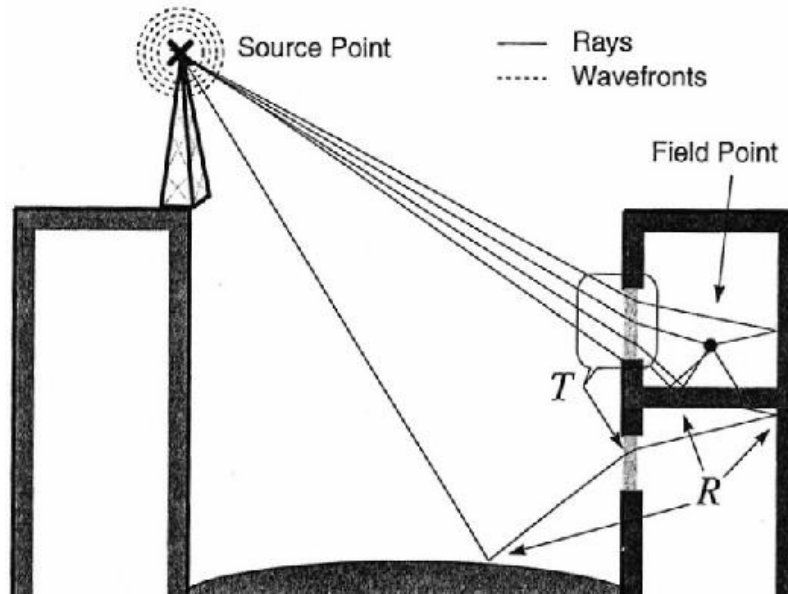
Figure 8.   Propagation mechanisms in real environment (From Ref. [11].)

2.   Geometric Theory of Diffraction

Geometrical optics, however, does not include the effects of ray diffractions caused by knife-edges and corners of structures in an urban environment. Keller devised the geometric theory of diffraction (GTD) to account for the diffractions [11]. Figure 9 shows a ray being diffracted from a wedge.
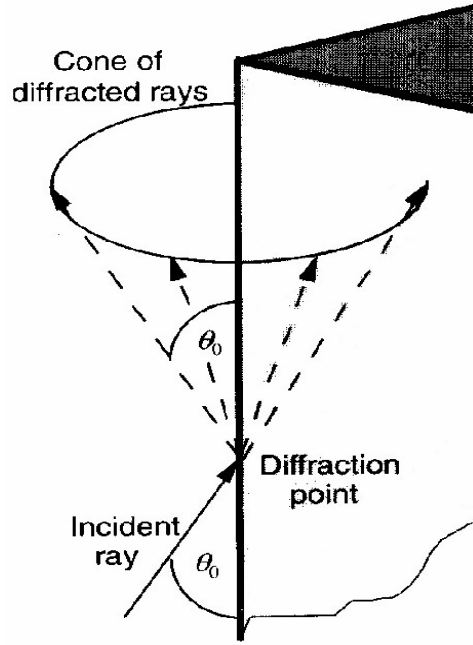
Figure 9.   Edge-diffracted rays according to GTD (From Ref. [11].)

The diffracted field is given as [11]

$$\mathbf{E}_d = \mathbf{D}\mathbf{E}_i A_d e^{-jkr} \tag{24}$$

where

$$\mathbf{E}_d = \begin{bmatrix} E_{d\parallel} \\ E_{d\perp} \end{bmatrix}, \; \mathbf{D} = \begin{bmatrix} D_\parallel & 0 \\ 0 & D_\perp \end{bmatrix}, \; \mathbf{E}_i = \begin{bmatrix} E_{i\parallel} \\ E_{i\perp} \end{bmatrix} \tag{25}$$

and

$$A_d = \begin{cases} 1/\sqrt{r} & \text{for plane or cylindrical wave incidence} \\ \sqrt{r_i/r(r+r_i)} & \text{for spherical wave incidence.} \end{cases} \tag{26}$$

Here, $E_{i\parallel}$ and $E_{i\perp}$ denote the electric field parallel and perpendicular components relative to the plane of incidence, respectively, while $E_{d\parallel}$ and $E_{d\perp}$ are the electric fields parallel and perpendicular to the plane of diffraction. Also, A_d is the spreading factor, r_i is the distance from the source to the diffracting edge, r is the distance from the diffracting edge to the field point, k is the wavenumber, and $D_\parallel$ and $D_\perp$ are the diffraction coefficients.

16

An extension of GTD is the uniform theory of diffraction (UTD) which provides more accurate prediction as it includes field points in the Fresnel-zone-like region close to the shadow boundary. Since UTD accounts for all points in space, it is more suitable for practical propagation applications [11].

Finally, the total field at an observation point, P, can be obtained as the sum of all the GO and GTD rays arriving at P [9]

$$\mathbf{E}_{\mathbf{T}}(P) = \mathbf{E}_{\mathbf{GO}}(P) + \mathbf{E}_d(P). \tag{27}$$

In this thesis, a ray tracing engine (Urbana) applies GO and GTD to model, simulate and predict the performance of UAV data links in an urban environment.

In this chapter, the concepts behind the mechanisms of radiowave propagation in complex urban environment were presented. These empirical and physical models can be used to describe the characteristics of radiowave propagation in an urban environment. Ray tracing is a useful tool for characterizing the radiowave propagation channel. A ray tracing engine was used for the modeling and simulation process in this thesis. However, before the simulations are presented, a summary of diversity techniques is given in the next chapter.

THIS PAGE INTENTIONALLY LEFT BLANK

III. DIVERSITY TECHNIQUES

Mobility is a fundamental feature of "untethered" communications networks [14]. The mobility of combat units is an essential attribute to combat effectiveness. Thus, there is great demand for mobile wireless communication systems in military applications. As discussed in the previous chapter, radio propagation in urban areas is subjected to multipath and fading that can severely degrade the quality of transmission and cause loss of a communications link. The challenge is how to ensure good and reliable radio communications connectivity without limiting operational flexibility.

The countermeasures for fading can be found in implementing diversity concepts. The basic theory of diversity is based on the fact that there is a low chance of independent fading signal paths experiencing the same fading, which means there is a good chance that one of the signal paths is not severely faded. Independent fading paths can be achieved by separating the signal in time, frequency, space, or polarization [14].

A. TIME AND FREQUENCY DIVERSITY

Time diversity is achieved by repeatedly transmitting the signal at a time spacing equal to or larger than the coherence time of the channel. Thus each received signal is subjected to independent fading. For example, in a CDMA RAKE receiver implementation, the RAKE receiver is able to align the multiple received signals in time so that a better estimation of the original signal may be obtained [15].

Frequency diversity means that the signal is transmitted using more than one carrier frequency with frequency spacings equal to or larger than the coherence bandwidth of the channel. Thus each received signal is at different carrier frequency, and is therefore subjected to independent fading [15].

Besides time and frequency diversity, there are other less commonly used techniques such as spatial diversity, cross polarization diversity and angle diversity. These were the focus of the research in this thesis.

B.   SPATIAL DIVERSITY

Spatial diversity can be achieved with multiple combinations of transmit or receive antennas in a radio system. Basically, the antennas are spaced sufficiently far apart to ensure de-correlation and independent fading of the transmit or receive signals from the antennas [10].

1.   Diversity on Receive

Independent fading paths in space are achieved using a receiving antenna array, where each element receives a separate path signal. The antenna elements are required to be spaced to ensure uncorrelated received signals.

Figure 10 shows the relationship between omni-directional antenna spacing and its covariance factor. For example, a 0.4λ spacing is enough to ensure uncorrelated fading between two omni-directional antennas. A separation between two antennas of one-half to one wavelength is considered sufficient to obtain two nearly uncorrelated signals [10].
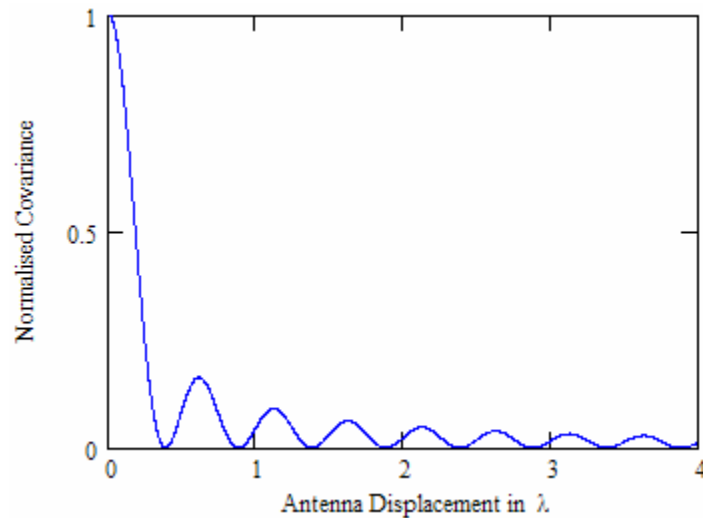
Figure 10.   Omni-directional Antenna Spatial Covariance (After Ref. [15].)

The larger the separation in wavelengths, the lower is the correlation between the received signals. It is important for antenna diversity that the received signal be uncorrelated and independent to ensure that there is a chance of stronger signal on one path if the other path is subjected to severe degradation [15].

20

Figure 11 shows the potential advantage of employing two antenna for receive diversity. With the antennas spaced $d \geq \lambda/2$ apart to ensure uncorrelated received signals, the Gaussian distributed received signals have cumulative distribution functions (CDFs) that show a diversity gain, that is, an improvement in the signal-to-noise ratio (SNR). A steep CDF is desirable. Using this advantage, the received signals can be combined using various techniques that can improve the receiver performance. The techniques are: (1) selection combining (SC), (2) maximal-ratio combining (MRC), and (3) equal-gain combining (EQC) [12].
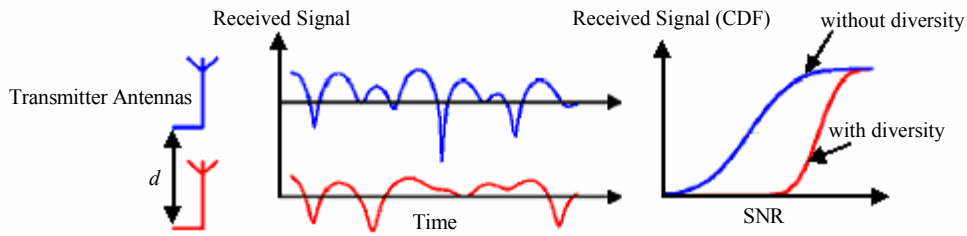
Figure 11.   Two antenna for receive diversity (After Ref. [10].)

In the SC method for two antennas, as shown in Figure 12, the branch with the maximum voltage SNR is selected as the contributing received signal. For example, branch one SNR_1 is chosen if it is larger than branch two SNR_2. The weaker branch will not be used. In this method, the mean SNR of the selected signal is [12]

$$\langle SNR \rangle = \Gamma \sum_{n=1}^{N} \frac{1}{n} \tag{28}$$

where Γ is the mean branch SNR. The mean SNR improves logarithmically with the N number of branches.
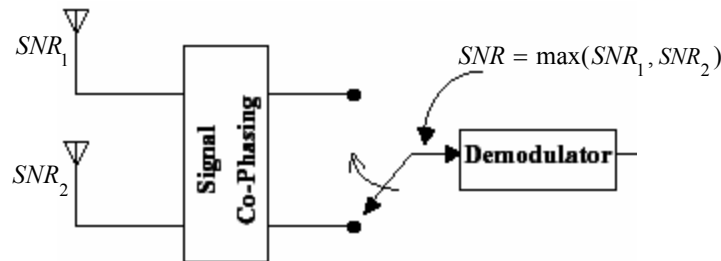
Figure 12.   Two branch selection combining (SC) with equal noise power (After Ref. [16].)

21

In the MRC method shown in Figure 13, each branch signal is first weighted by its received instantaneous voltage SNR, $r_1/\sqrt{N}$ and $r_2/\sqrt{N}$, respectively. Thus the branch with the higher voltage SNR is weighted more than the branch with lower voltage SNR. The weighted signals are then co-phased and coherently added. This method yields the highest instantaneous SNR possible with any linear combining technique. However, implementation of the MRC is expensive since the weights need both amplitude and phase tracking of the channel response [12].
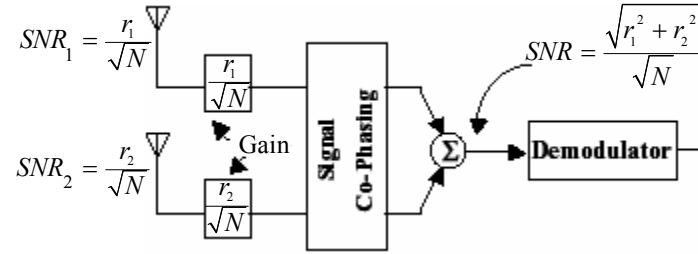
Figure 13.   Two branch maximal-ratio combining (MRC) with equal noise power (After Ref. [16].)

The mean SNR at the output of the combiner is [12]

$$\langle SNR \rangle = \sum_{n=1}^{N} \Gamma = N\Gamma \tag{29}$$

where Γ is the mean branch SNR. The mean SNR improves with the number of branches, N.

In the EQC method, the weights have the same constant magnitude, G, unlike the MRC, where the weights are based on the instantaneous voltages. As shown in Figure 14, the weighted signals are then co-phased and coherently added. The noise power for the output voltage SNR is doubled.
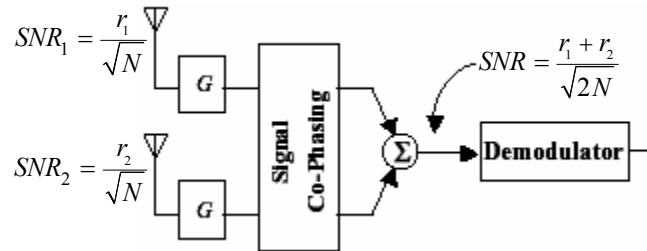
Figure 14.   Two branch equal gain combining (EGC) with equal noise power (After Ref. [16].)

The closed-form expression for the mean SNR at the output of the combiner is [12]

$$\langle SNR \rangle = \left[1+(N-1)\frac{\pi}{4}\right]\Gamma \qquad (30)$$

where Γ is the mean branch SNR. The mean SNR improvement is less than the MRC improvement.

From Figure 15, the plots of the improvement to the mean SNR show that the MRC and EQC have better improvement gain than the SC method. For larger N, the MRC is about 1 dB better than the EQC method.
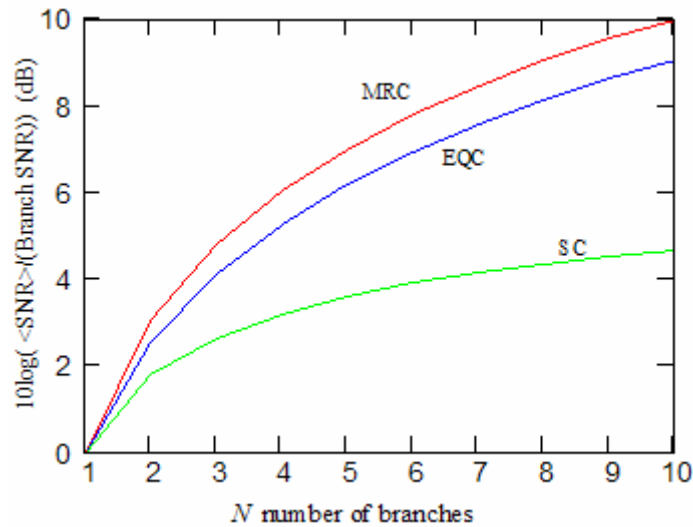
Figure 15.   Improvement in mean SNR for various combining techniques (After Ref. [12].)

2.   Diversity on Transmit

For transmit diversity, as shown in Figure 16, the transmitter power is split between the antennas. With the antennas being spaced $d \geq \lambda/2$ apart to ensure uncorrelated received signals, the received signal strength (SNR) which is averaged over all angles does not improve, but the variance of the signal is reduced [10].

23
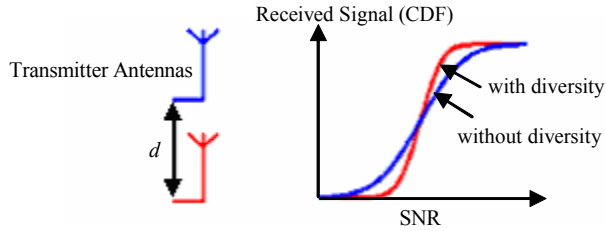
Figure 16.   Two antenna for transmit diversity (After Ref. [10].)

The advantage in SNR improvement of diversity on transmit might not be as significant as diversity on receive but it has its important use in the multiple input, multiple output (MIMO) concept. With multi-element antenna (MEA) arrays employed at both the transmitter and receiver ends, multipath in a rich scattering environment can be employed via space-time processing to achieve very high spectral efficiencies [12]. Figure 17 shows the capacity efficiency for MIMO arrays.
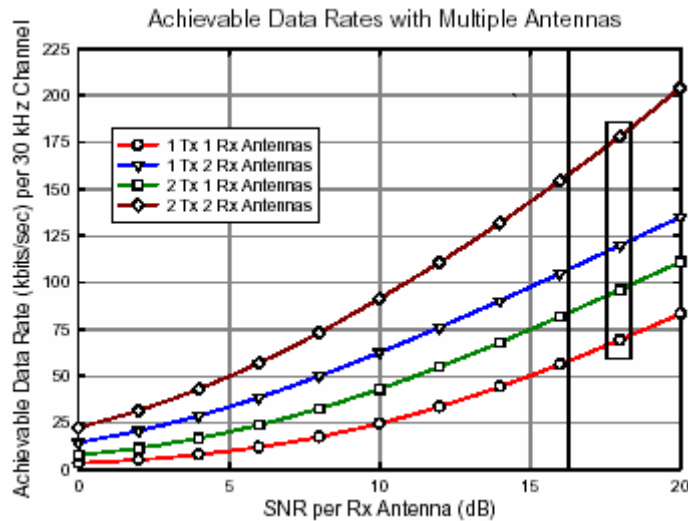
Figure 17.   Capacity efficiency with multiple antennas (After Ref. [17].)

It can be observed that for a SNR per receiver antenna of about 17 dB (boxed location) in a 30 kHz channel, a single antenna transmit-receive pair (red plot) can achieve a data rate of about 70 kbps, while a two antennas transmit-receive pair (brown plot) can achieve a data rate of about 175 kbps. There is an improvement of 2.5 times in data rate capacity.

C.   POLARIZATION DIVERSITY

In addition to spatial diversity, the use of orthogonal polarizations to exploit polarization diversity is another approach. This approach provides for only two diversity branches. Orthogonally polarized antennas ensure de-correlation of the two channels [15].

Figure 18 shows the concept of polarization diversity. A horizontal antenna receives only horizontally polarized waves. Likewise, a vertical antenna receives only vertically polarized waves. In this approach, two antenna dipoles can be co-located, whereby one dipole is orientated vertically and the other horizontally. These orthogonal antennas are co-located to save space. This technique is also known as dual-polarization.
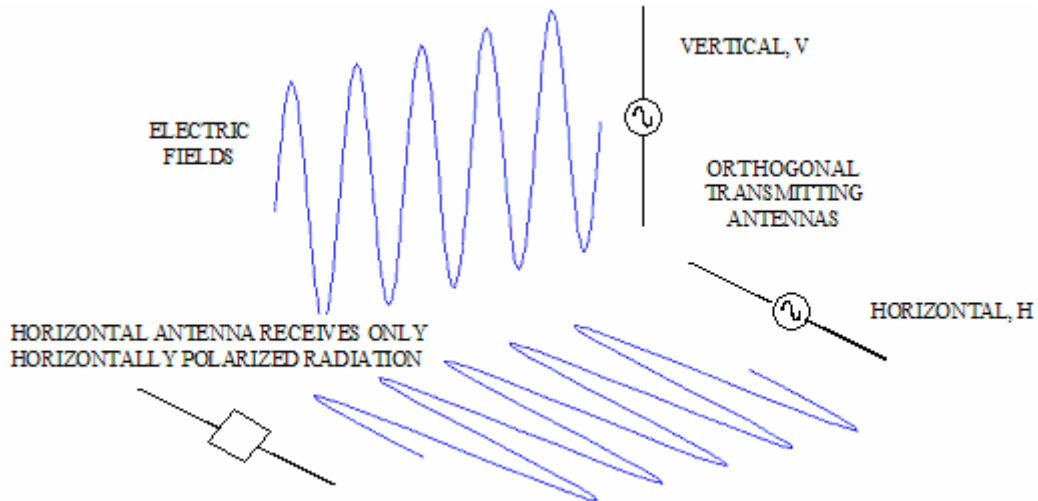
Figure 18.   Polarization of waves generated by orthogonal linearly-polarized antennas

D.   ANGLE DIVERSITY

Another diversity technique is the use of directional antennas to achieve angular diversity. This approach is the basis of space-division multiple access (SDMA). Angle diversity or SDMA can result in an increase of spectral efficiency and capacity [18].

Directional antennas have larger gains and narrower beamwidths when compared to an omni-directional antenna. They enable the transmitter to steer the antenna beam towards the location of the intended receiver. At the same time, the directional antenna also reduces reception by another receiver or even interference by another transmitter, thus

providing a low probability of detection (LPD) system. With directional antennas having sector patterns, the same frequency and/or time slot can be used in each sector, as a result more users can operate in the same spectrum, improving the system capacity [18].

Figure 19 shows the concept of SDMA with directional antennas. With the transmitter steering the antenna beam (blue pattern) towards User 1, it reduces reception and interference by User 2, as it is located in the null of the antenna beam. Similarly, when the antenna beam (yellow pattern) is steered towards User 2, User 1 has no reception and provides no interference. Basically, SDMA improves system capacity and signal strength for both transmitter and receiver, at the same time it reduces the effect of interference.
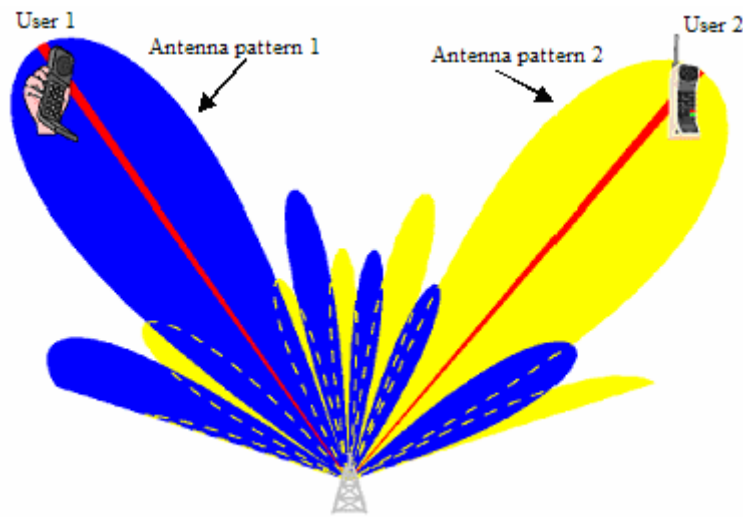
Figure 19.   Directional antennas—SDMA (From Ref. [10].)

In this chapter, the concepts behind the three diversity techniques of (1) spatial diversity, (2) polarization diversity, and (3) angle diversity or SDMA, were discussed. These diversity techniques were applied in the modeling and simulation of radiowave propagation in an urban environment. The purpose was to investigate the effects of diversity on the performance of urban radiowave links. The next chapter describes the software tool used in the modeling and simulation.

IV. MODELING USING URBANA

A. RAY TRACING WITH URBANA

The ray tracing software, Urbana Wireless Toolkit, from Science Applications International Corporation (SAIC), was used to model and simulate the effects of diversity on urban radiowave links. It is a computational electromagnetic (CEM) tool utilizing a ray tracing engine that combines physical optics, geometric optics, and diffraction physics to produce a 3-D simulation for radiowave propagation [19].

The deterministic ray tracing techniques of Urbana can be used to characterize radiowave propagation in an urban environment. Urbana uses ray tracing applied to CAD models for buildings, and other major features. The ray tracing engine would interrogate the 3-D geometry of the environment to provide inputs to the physical models for reflection, diffraction around buildings and terrain, etc. [19].

For urban radiowave propagation modeling, the input parameters for Urbana are CAD facet models for the buildings and roads, including its surface material (e.g., concrete, earth, glass and dielectric properties). The other inputs are the placement, strength, and antenna patterns of transmitters and receivers. The outputs are composite signal strength, angle of arrival and time delay of each arriving signal ray at each receiver or observation point [19].

B. URBAN CITY MODEL

In this thesis, a small urban city model adapted from an existing Urbana Wireless Toolkit model was used. The Urbana model was a replica of downtown Austin, Texas. A view of the city model is shown in Figure 20.
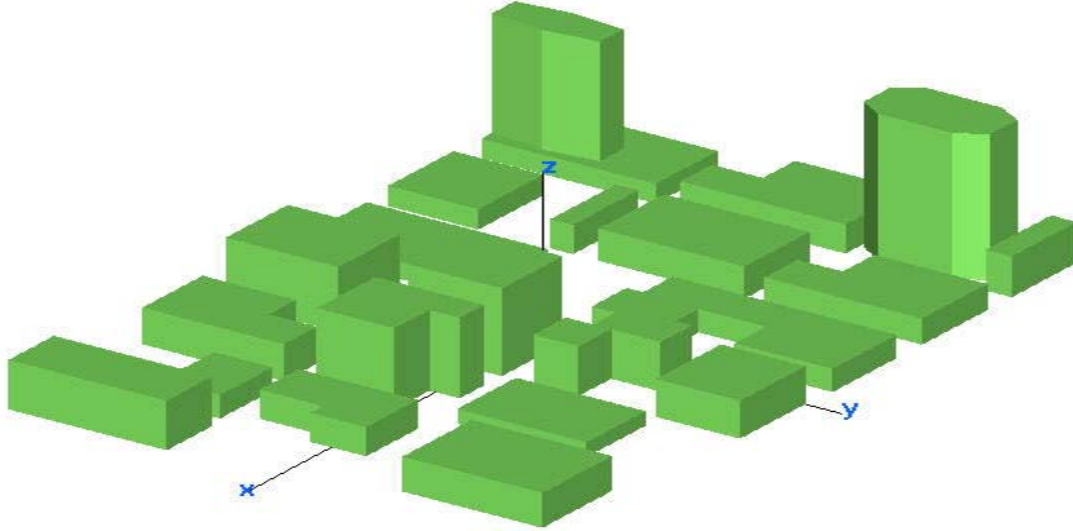
Figure 20.   Small city model without ground plane

The city model occupies a box area of 600 m by 400 m by 150 m. The tallest building is at a height of 150 m. There are 23 separate buildings in the model.

1.   Building Materials

Previous calculations by Lock [20] and Pala [21] investigated the effects of various building materials on UAV data links. The outdoor signal levels are not all that sensitive to the building materials as long as all of the buildings are not completely perfect electric conducting (PEC). Therefore, since the evaluation of diversity techniques was the goal of this research, all the buildings were modeled with the same material.

In Urbana modeling, the 23 blocks of building are made up of 314 facets with material parameters stated in Table 2. Each concrete facet is a penetrable layered slab with air backing.

COATING MATERIAL	RELATIVE PERMITTIVITY		RELATIVE PERMEABILITY		RESISTIVITY	THICKNESS
	ε'	ε''	μ'	μ''	ρ (ohm)	t (m)
Concrete	10.1	0.5	1.0	0	10^{30}	0.3

Table 2.   City model building material

2. Building Edges

Besides modeling the building surfaces, the edges of each building are also included in Urbana, as shown in Figure 21. The purpose of the edges is to account for the various radiowave diffractions, which occur from building and rooftop edges.
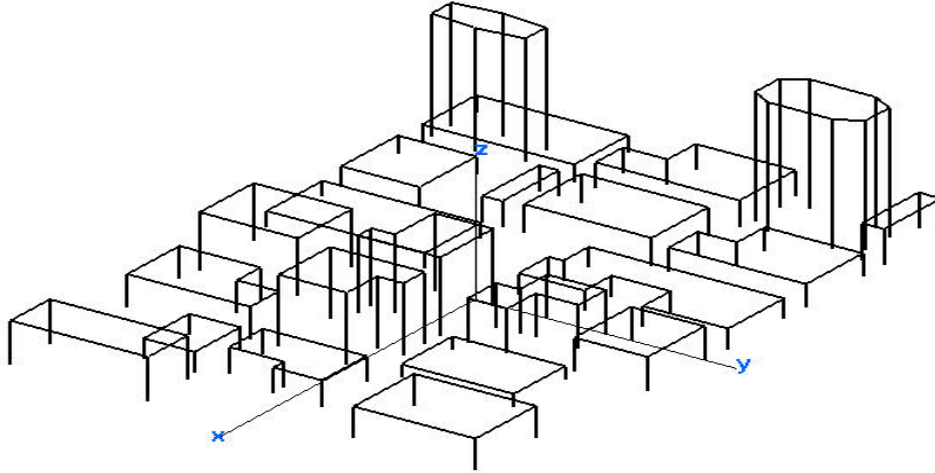
Figure 21. Building edges in the small city model

3. Ground Plane

A semi-infinite ground plane is included with the city model. The city model basically resides on a semi-infinite ground plane as shown in Figure 22, which accounts for ground reflections. The ground plane has $\varepsilon' = 3$ and $\mu' = 1$.
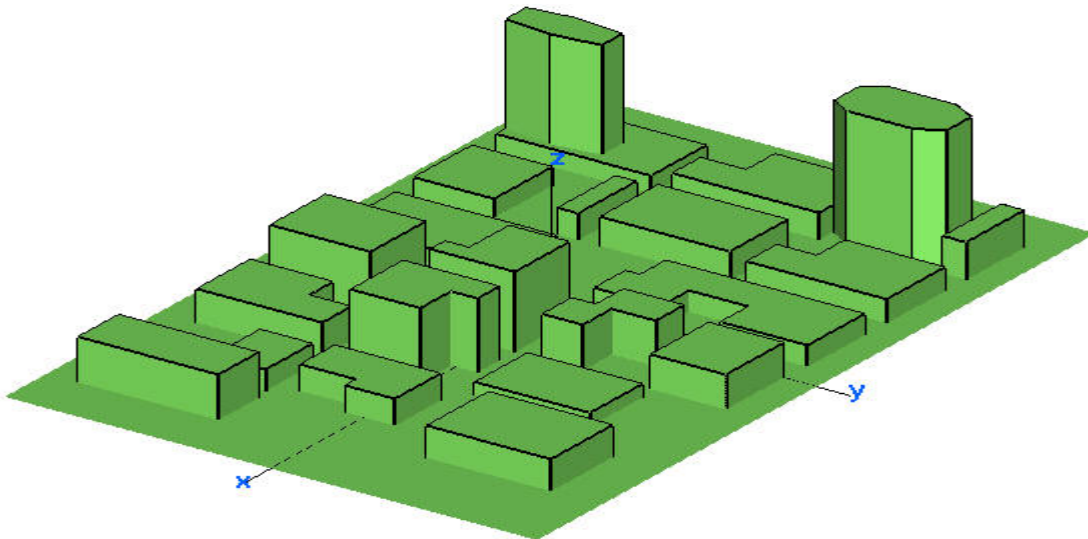
Figure 22. Small city model with edges and ground

C. URBANA USER INPUT PARAMETERS

In order for Urbana to model and simulate the characteristics of radiowave propagation in any environment, there are a number of parameters that the user needs to provide.

Table 3 shows a list of some user input parameters for Urbana and their sample values. An entire user input file is listed in Appendix A. The settings in Table 3 were used throughout the simulations. The transmitter and receiver antennas can be modeled as dipoles or by using an antenna pattern data file describing a typical radiation pattern. The modeling of the antennas is dependent on the type of scenario to be simulated.

PARAMETERS	SETTINGS
Scatterer model	*citywgrnd.facet*
Length unit	meters
Frequency	900 MHz
Tx antenna	dipole or antenna pattern data
Rx antenna	dipole or antenna pattern data
Ray tracing computation	geometrical optics (GO)
Edge diffraction	uniform theory of diffraction (UTD)
Edge model	*city.edge*
Burst ray angular spacing	2°
Maximum ray bounces	7
Coating material	from Table 2
Advance features	off

Table 3.   Urbana user input parameters

D. MODELING OF ANTENNAS

The characteristics of the transmitting and receiving antennas are essential parameters for the Urbana processing. Basically, different types of antennas affect radiowave propagation differently through their radiation patterns. There were two basic types of antennas modeled in this thesis, discussed in the following sections.

1.   Dipole Antenna

The $\lambda/2$ dipole is the basic antenna element used throughout this thesis. The radiation pattern of a $\lambda/2$ z-directed dipole at an operating frequency of 900 MHz in the xz plane is shown in Figure 23. It has an omni-directional pattern in xy plane.
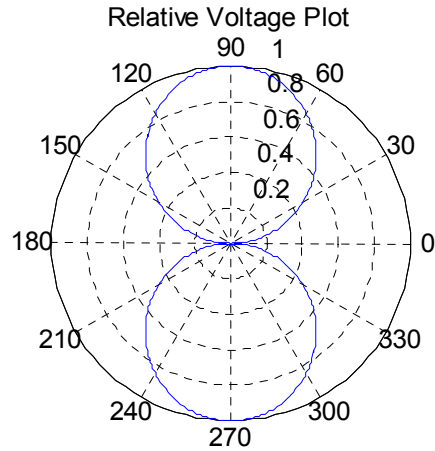
Figure 23.   Half-wave dipole radiation pattern in xz plane

2.   Directional Antenna

A directional antenna pattern was created for use in Urbana. Figure 24 shows a plot of the radiation pattern. It has a 3-dB half-power beamwidth (HPBW) of 10° at an operating frequency of 900 MHz. The radiation into the rear hemisphere was set to zero, because it was assumed that this pattern is due to an array of elements with a cavity or ground plane backing. The directivity of the directional antenna is about 25 dB.
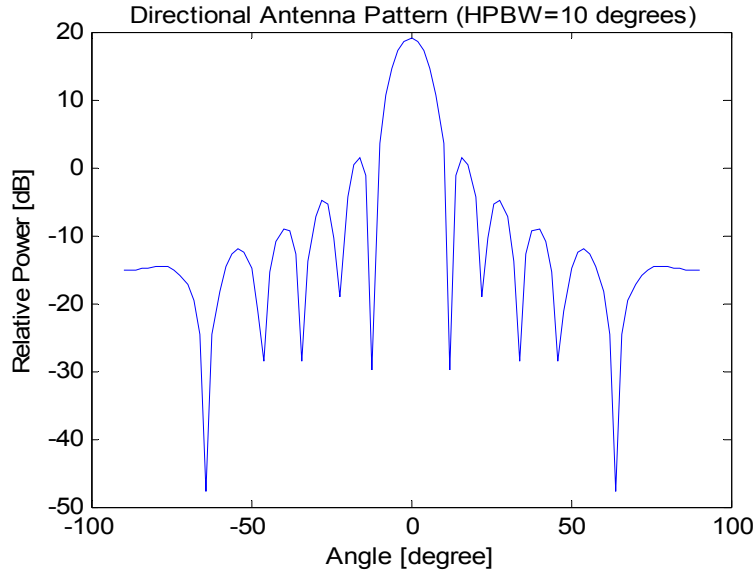
Figure 24.   Directional antenna radiation pattern with HPBW=10°

In Urbana, an antenna pattern file containing the linear field strength components of the above directional antenna was created. The pattern file is generated using the Matlab codes shown in Appendix B. The pattern is normalized to the directivity, which is automatically computed by Urbana. Figure 25 shows the free space radiation pattern simulated in Urbana with an excitation of 1 W, and pointed in the direction of angles $\phi = 0°$ and $\theta = 90°$, respectively. The location of the antenna is at $(x, y, z) = (-10$ m, -55 m, -150 m). The observation plane is at a height of $z = 4$ m.
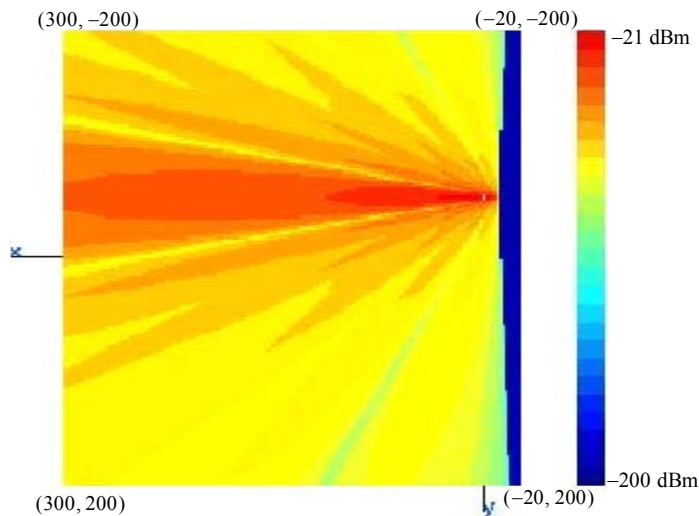
Figure 25.   Signal coverage in the forward hemisphere of the directional antenna at location $(-10$ m, -55 m, 150 m)

32

E. MODELING OF DIVERSITY TECHNIQUES FOR UAV COMMUNICATIONS LINKS

With an appreciation of the UAV operations and the critical need for effective tactical communications, we now explore methods of implementing various diversity techniques to improve the effectiveness of UAV communication links in MOUT. This also sets the framework for simulations later on.

1. Spatial Diversity

In order to investigate the benefit of antenna spatial diversity, two antennas were considered in the simulations. Further improvement is achievable with four, eight or even more antennas, but at the expense of increased antenna area ("real estate").

a. Spatial Diversity on Receive

In the Urbana modeling process, a vertical $\lambda/2$ dipole was modeled as transmitting from a UAV hovering 150 m above the city center, as shown in Figure 26. The UAV structure itself was not considered. It was assumed that the dipole type pattern is achieved when the antenna is installed on the UAV.
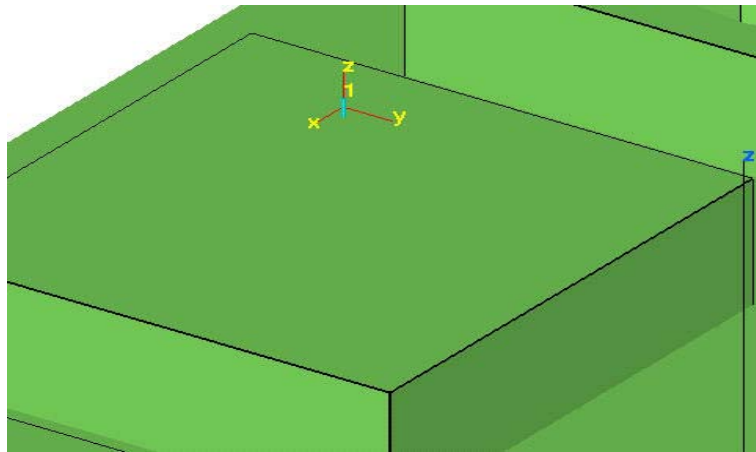
Figure 26.   Vertical $\lambda/2$ dipole transmitting at location $(-10 \text{ m}, -55 \text{ m}, 150 \text{ m})$

On the ground, observation points were located at a height of 1.5 m above the ground plane and covered the 600 m by 400 m small city model with cell size of 2 m.

Some of these observation points were designated as receivers with $\lambda/2$ dipoles for detailed analysis.

After the simulations, spatial diversity on receive was assessed by analyzing the signal strength obtained at the receivers. A two-antenna diversity approach on receive can be evaluated by analyzing a pair of the $\lambda/2$ dipoles which are placed 2 m apart. The dipole separation is more than 10λ apart at the operating frequency of 900 MHz. This ensures good de-correlation between the received signals. Additional simulations and analysis with different orientations of the transmitting and receiving dipoles were also investigated.

b.   *Spatial Diversity on Transmit*

In modeling the spatial diversity on transmit, a pair of $\lambda/2$ dipoles were modeled on the transmitting UAV. The dipoles were placed at $\lambda/2$ apart (0.167 m at 900 MHz) to ensure sufficient de-correlation of the transmit signals. Figure 27 shows the spatial diversity model on transmit. In addition, the total excitation power for the pair of dipoles was 1 W. Thus each dipole transmits 0.5 W. As a result, there is a common basis for comparison with a single dipole transmitter excited by 1 W.
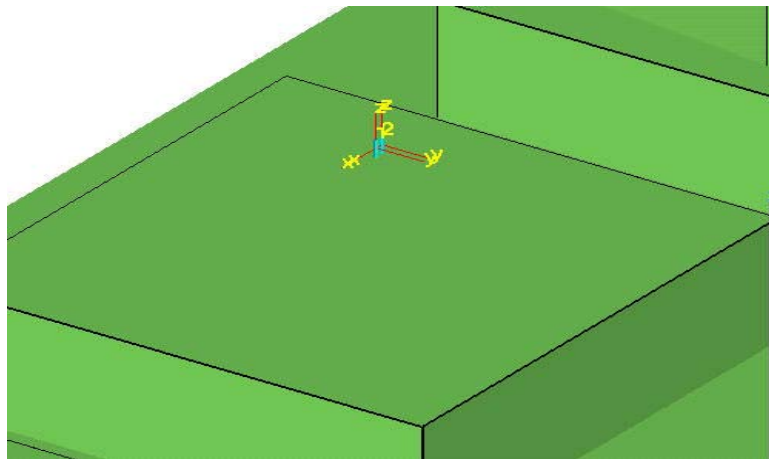
Figure 27.   Spatial diversity on transmit: two vertical dipoles at locations
$(-10 \text{ m}, -55 \text{ m}, 150 \text{ m})$ and $(-10.167 \text{ m}, -55 \text{ m}, 150 \text{ m})$

On the ground, observation points were located at a height of 1.5 m above the ground plane and covered the 600 m by 400 m small city model with cell size of 2 m. Some of these observation points are designated as receivers with $\lambda/2$ dipoles for detailed analysis. The advantage of having spatial diversity on both transmit and receive was investigated by analyzing the total received signal strength.

2.   Polarization Diversity

In modeling polarization diversity, there were two orthogonal transmit dipoles in co-location. One antenna was vertically polarized while the other was horizontally polarized, as shown in Figure 28. This is also referred to as dual-polarization diversity.
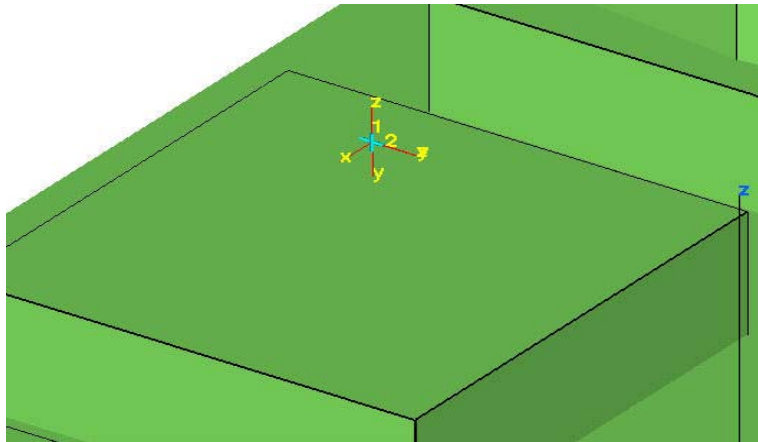
Figure 28.   Dual-polarization diversity on transmit at location $(-10\text{ m}, -55\text{ m}, 150\text{ m})$

On the ground, observation points were located at a height of 1.5 m above the ground plane and covered the 600 m by 400 m small city model with cell size of 2 m. Some of these observation points are designated as receivers with $\lambda/2$ dipoles for detailed analysis. The receiver antennas are $\lambda/2$ dipoles orientated either vertically, horizontally, or both. Analysis was conducted by comparing the performance of polarization diversity to the spatial diversity approach described previously.

3.   Angle Diversity

In order to demonstrate angle diversity, a vertical $\lambda/2$ dipole was used as the transmitting antenna on the UAV. A receiver with a directional antenna pattern (shown in

Figure 25) was located on the ground. For angle diversity analysis, a few transmitting dipole locations were selected and transmissions from the UAV simulated. This represents samples of transmissions along a UAV flight path. For the receiving antenna on the ground, a shadow location was chosen at a point with deep fading. The receiving directional antenna was steered towards the direction of the strongest incoming signal, which is generally not in the unobstructed line-of-sight direction. In addition, a comparative analysis was done for all of the diversity techniques described previously, to assess their relative performance in the urban environment.

In this chapter, the framework for the simulation process was defined. The city model and the different types of antennas to be used were created and modeled. Also, the scenarios for applying the diversity techniques to the UAV data links over the urban city were also described. The next chapter presents the simulation results.

V. SIMULATIONS AND ANALYSIS

A. SIMULATIONS OF SPATIAL DIVERSITY

Antenna spatial diversity was simulated by using two $\lambda/2$ dipoles. Antenna spatial diversity can be simulated on either receive, or transmit, or both. On transmit, antennas were placed $\lambda/2$ apart (0.167 m at 900 MHz) to ensure de-correlation of the receive signals.

1. Spatial Diversity on Receive

A UAV transmitter was modeled as a single dipole transmitting over the city model. The observation points for receiving signals were positioned throughout the city area of 600 m by 400 m with cell size of 2 m, and at a height of 1.5 m. A single $\lambda/2$ dipole antenna was modeled as receiver in some of the observation cells for analysis. Also, vertical (V) and horizontal (H) orientations of the transmitting and receiving dipoles were considered. Note that vertical dipoles are parallel to the z axis, while horizontal dipoles are parallel to the y axis. Table 4 shows the parameters used in the simulation.

PARAMETERS	SETTINGS
Operating Frequency	900 MHz
Type of Tx antenna	dipole
Length of Tx antenna	0.1667 m
Location of Tx antenna	$(x, y, z) = (-10 \text{ m}, -55 \text{ m}, 150 \text{ m})$
Tx power/phasing	$1\angle 0°$ W
Orientations of Tx antenna	parallel to the z axis /or parallel to the y axis
Observation points (used for signal coverage plot computation)	600 m by 400 m with cell size of 2 m, height of 1.5 m
Type of Rx antenna	dipole
Length of Rx antenna	0.1667 m
Locations of Rx antenna	$(145 \text{ m}, 200 \text{ m}, 1.5 \text{ m})$ to $(145 \text{ m}, -200 \text{ m}, 1.5 \text{ m})$ with 2 m resolution
Orientations of Rx antenna	parallel to the z axis /or parallel to the y axis

Table 4.   Urbana input parameters for simulation of spatial diversity on receive

The total signal strength coverage plots are shown in Figures 29 through 31. Urbana computes the total electric field strength of all arriving signal rays at each observation point to plot out the total signal strength in dBm.

Figures 29 and 30 illustrate the signal coverage over the city for a vertical transmitting dipole. Figure 29 shows the 3-D view with building edges. The location of the transmitting antenna is marked by the symbol "X" in Figure 30. In the urban environment, the presence of buildings results in multipath. Thus, there are locations where fading is dominant due to the various mechanisms discussed in Chapter II. This can be observed in the variation of the signal strengths which are represented by the different color codes. The strongest received signal is about -21 dBm and weakest is -82 dBm.
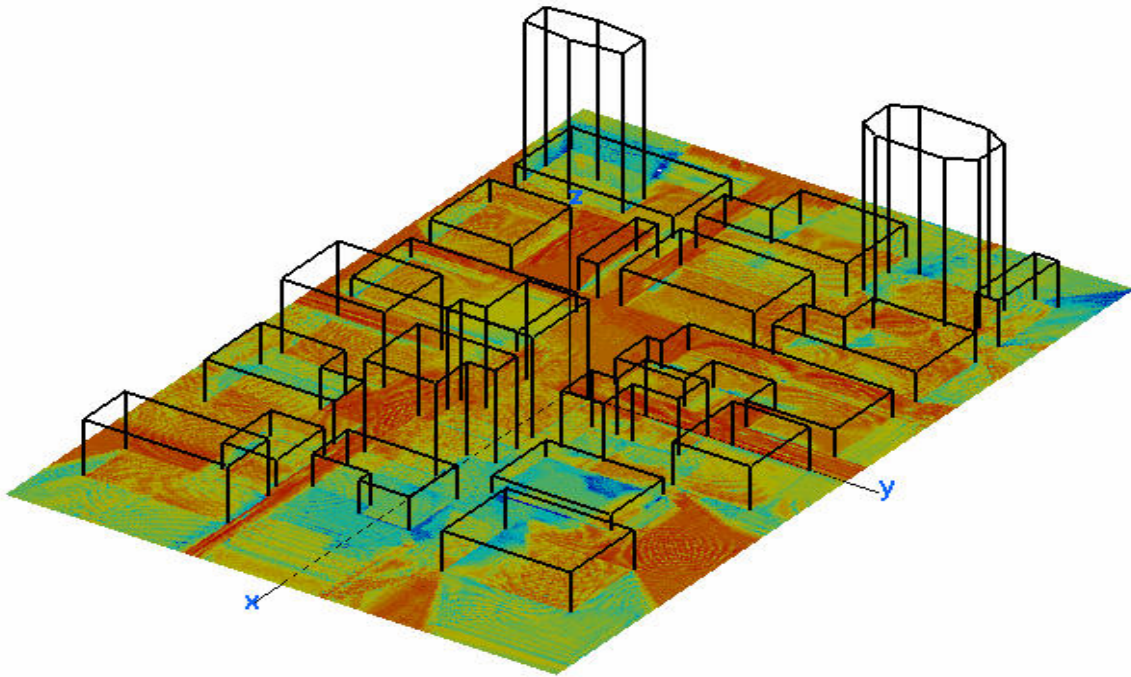
Figure 29.　Signal coverage (3-D view with building edges) for a vertical transmit dipole at location $(-10 \text{ m}, -55 \text{ m}, 150 \text{ m})$
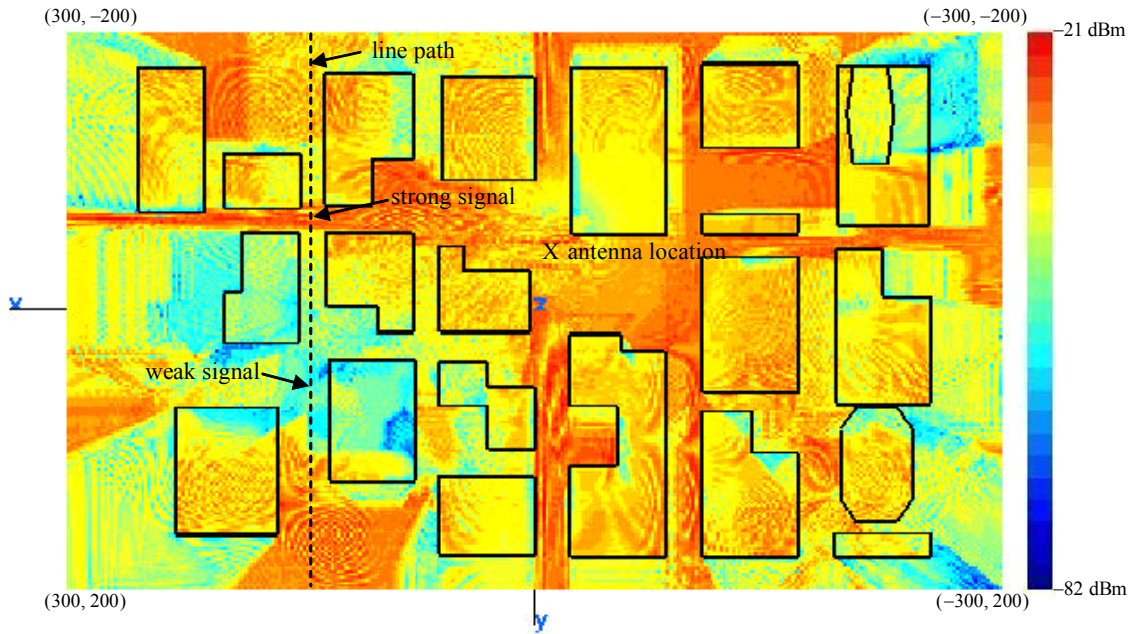
Figure 30.   Signal coverage for a vertical transmit dipole at location
$(-10\ \mathrm{m}, -55\ \mathrm{m}, 150\ \mathrm{m})$

The total signal strength coverage with a horizontal transmitting dipole, shown in Figure 31, ranges from a strongest received signal of about -14 dBm to a weakest of about -80 dBm. The stronger signals have larger values than those for the vertical transmitting dipole. However, the stronger signals are concentric near and under the transmitter location because the horizontal dipole has a downward radiation at the antenna location. A vertical dipole has a null pointing downward. Horizontal radiation is not as far reaching as vertical radiation most likely due to the large number of vertical edges, which enhances edge diffraction.

(300, 200)   (300, −200)

−14 dBm

(−300, −200)   (−300, 200)

−80 dBm

Figure 31.   Signal coverage for horizontal transmit dipole at location
(−10 m, −55 m, 150 m)

In order to establish a common basis for comparing the different diversity techniques, observation points from (145 m, 200 m, 1.5 m) to (145 m, −200 m, 1.5 m) at 2 m resolution on the *y* axis were used. This is called a line path in Urbana, and is shown by the dashed line in Figure 30. There are 200 observation points on this path. It was chosen because the reception is strong at some points and experiences deep fading at others. Each observation point was modeled with a dipole and receiver.

Figure 32 compares the difference between a vertical dipole transmitter and receiver pair (VTVR) to a horizontal dipole transmitter and receiver pair (HTHR). It is observed that at locations near to the transmitter (observation points 50 to 125), the horizontal dipole pair has higher received signal strength as compared to the vertical dipole pair. At locations farther away (observation points 0 to 50 and 125 to 200), the vertical dipole pair has better performance. There are some deep fades encountered in the horizontal case due to blockage by buildings. The horizontal transmitting dipole has strong radiation toward the ground below the antenna location. Since the pattern nulls are pointed outward toward the horizon, the horizontal radiation is not as far reaching as a vertical transmitting dipole in these directions.
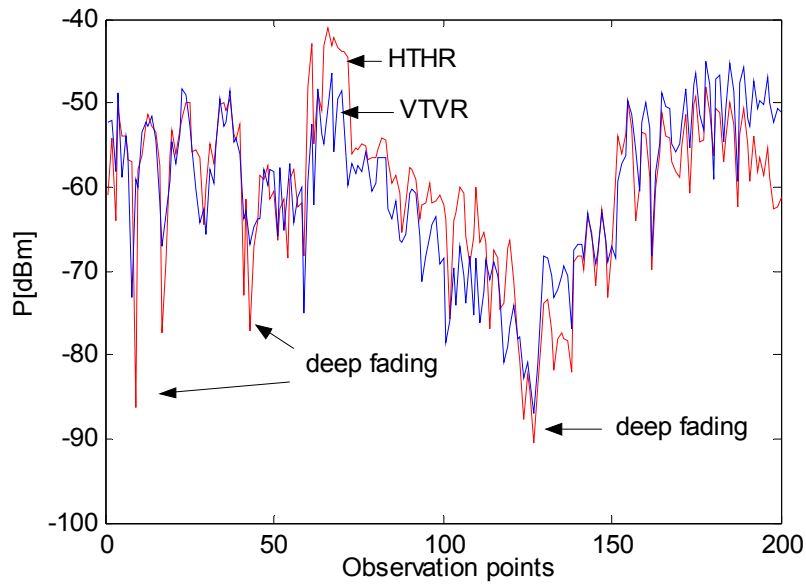
Figure 32.   Comparison between vertical and horizontal polarized links from the UAV to the ground

Figures 33 and 34 show the results for two receiving dipoles in each case. The signal power for receive spatial diversity was computed using the EGC diversity technique (discussed in Chapter III). For the EGC diversity technique, the received signal from each dipole was normalized by a constant gain, and then co-phased and coherently added to give a better signal strength.
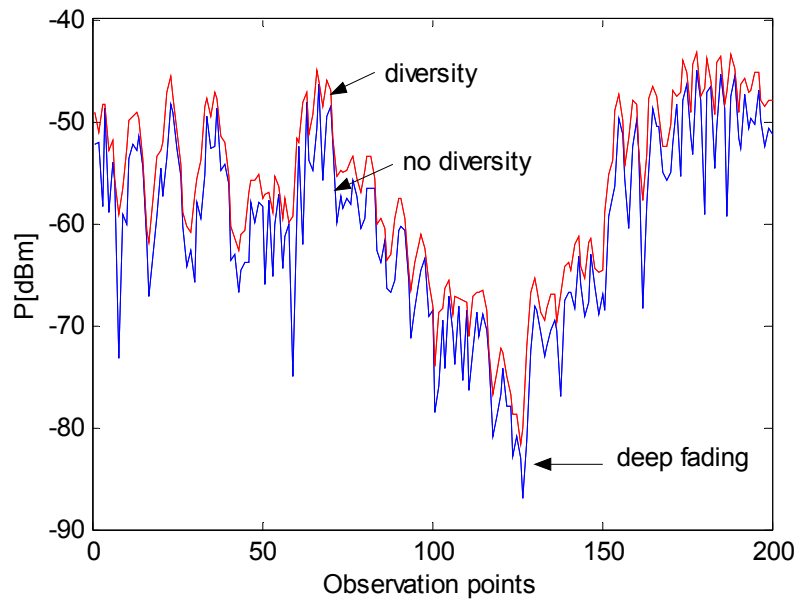
Figure 33.   Spatial diversity on receive, vertical case: diversity vs. no diversity

41
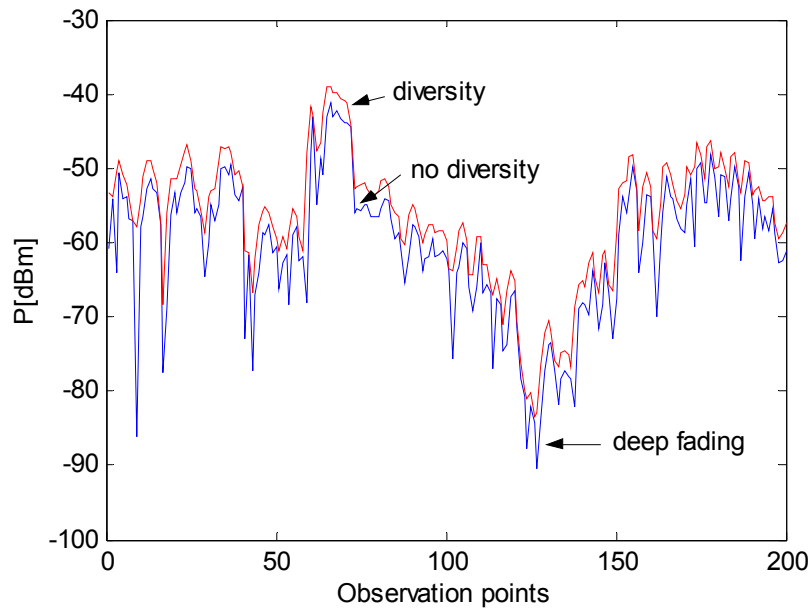
Figure 34.   Spatial diversity on receive, horizontal case: diversity vs. no diversity

The improvement using spatial diversity is obvious. The improvement factor for diversity on receive varies depending on location. At a location of deep fading, the improvement in received signal strength for both vertical and horizontal spatial diversity is about 6 dB, as compared to no diversity. It is to be noted that with EGC at the receivers, noise power would also be doubled (3 dB), so the SNR improvement would only be 3 dB. In both cases, spatial diversity has also reduced the number of drastic drops in signal strength (fading), which occur regularly along the observation points in the no diversity scenario.

Figure 35 shows the comparison between a vertical dipole transmitter and two vertical dipoles receiver on diversity (VTRD), to a horizontal dipole transmitter and two horizontal dipoles receiver on diversity (HTRD). The major difference is at observation points near to the transmitting location (50 to 125). The horizontal case has better received signal power. However, at locations far away from the transmitter (125 to 200), the vertical case has some improvement over the horizontal dipoles.
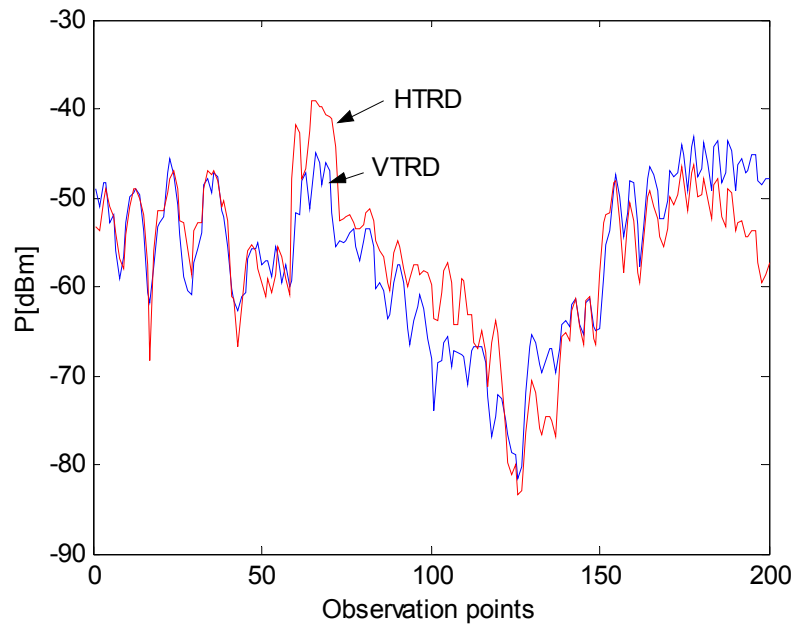
Figure 35. Spatial diversity on receive: comparison between vertical and horizontal cases

2. Spatial Diversity on Transmit

In this scenario, the transmitter uses antenna spatial diversity. At the transmitter, two vertical $\lambda/2$ dipoles were placed at $\lambda/2$ apart (0.167 m at 900 MHz), with each being excited by a zero-phase half unit power. Each dipole transmitted independently. Also, vertical and horizontal orientations of the transmitting and receiving dipoles were simulated. The parameters used in the simulation are shown in Table 5.

PARAMETERS	SETTINGS
Operating Frequency	900 MHz
Type of Tx antenna	2 dipoles
Length of Tx antenna	0.1667 m
Locations of Tx antennas	$(-10$ m, -55 m, 150 m) and $(-10.167$ m, -55 m, 150 m)
Tx power/phasing	$0.5\angle 0°$ W and $0.5\angle 0°$ W
Orientations of Tx antennas	parallel to the z axis /or parallel to the y axis
Observation points (used for signal coverage plot computation)	600 m by 400 m with cell size of 2 m, height of 1.5 m
Type of Rx antenna	dipole
Length of Rx antenna	0.1667 m
Locations of Rx antennas	$(145$ m, 200 m, 1.5 m) to $(145$ m, -200 m, 1.5 m) with 2 m resolution
Orientations of Rx antennas	parallel to the z axis /or parallel to the y axis

Table 5.   Urbana input parameters for simulation of spatial diversity on transmit

The total signal strength coverage plots are shown in Figures 36 and 37. Figure 36 provides the signal coverage over the city for the vertical transmitting dipoles. Considering all the observation points, the strongest received signal is -18 dBm and the weakest is -87 dBm. By comparing this with the level obtained with a single transmitting dipole, the strongest signal improves by about 3 dB. The signal strength coverage with the horizontal transmitting dipoles, as shown in Figure 37, ranges from the strongest received signal of about -13 dBm to the weakest of about -85 dBm.
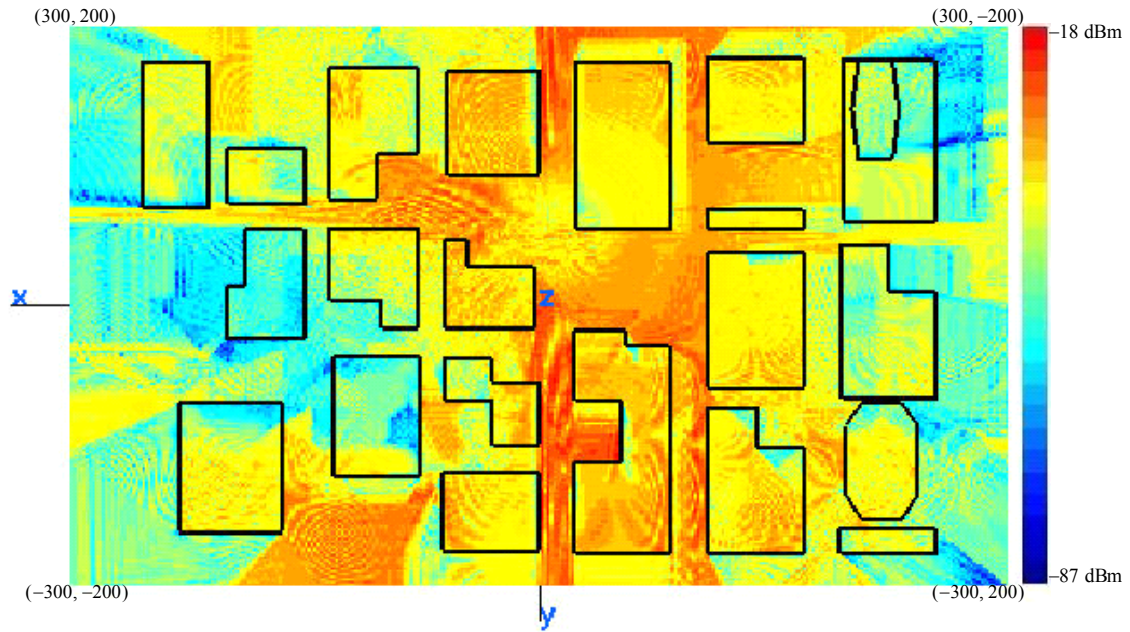
Figure 36.   Signal coverage for two vertical transmit dipoles at locations
$(-10 \text{ m}, -55 \text{ m}, 150 \text{ m})$ and $(-10.167 \text{ m}, -55 \text{ m}, 150 \text{ m})$
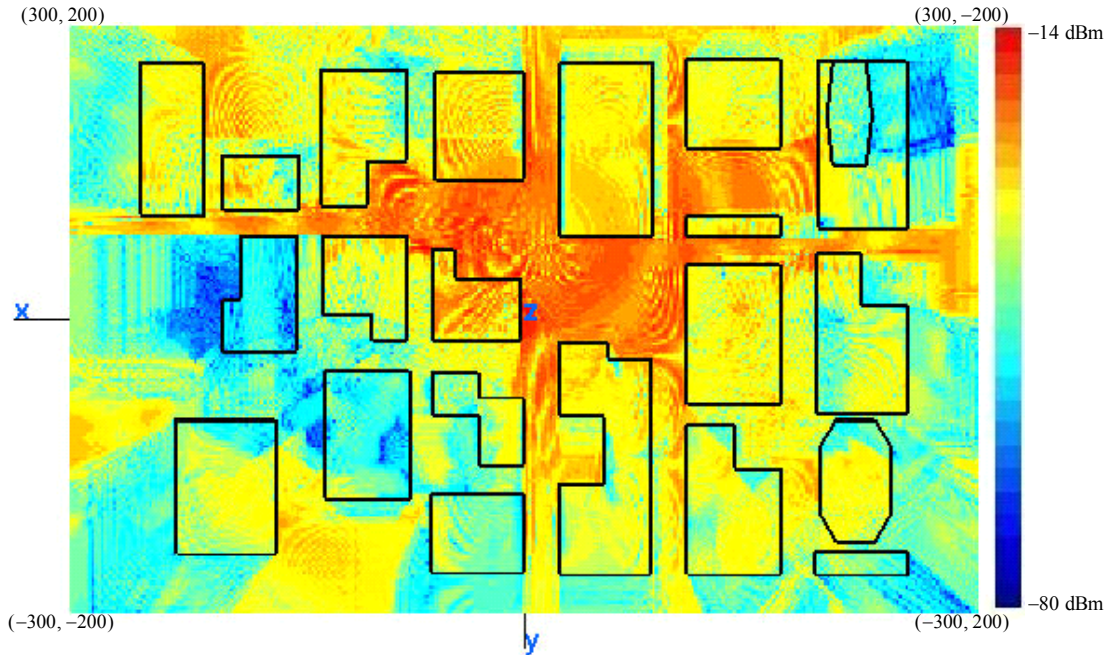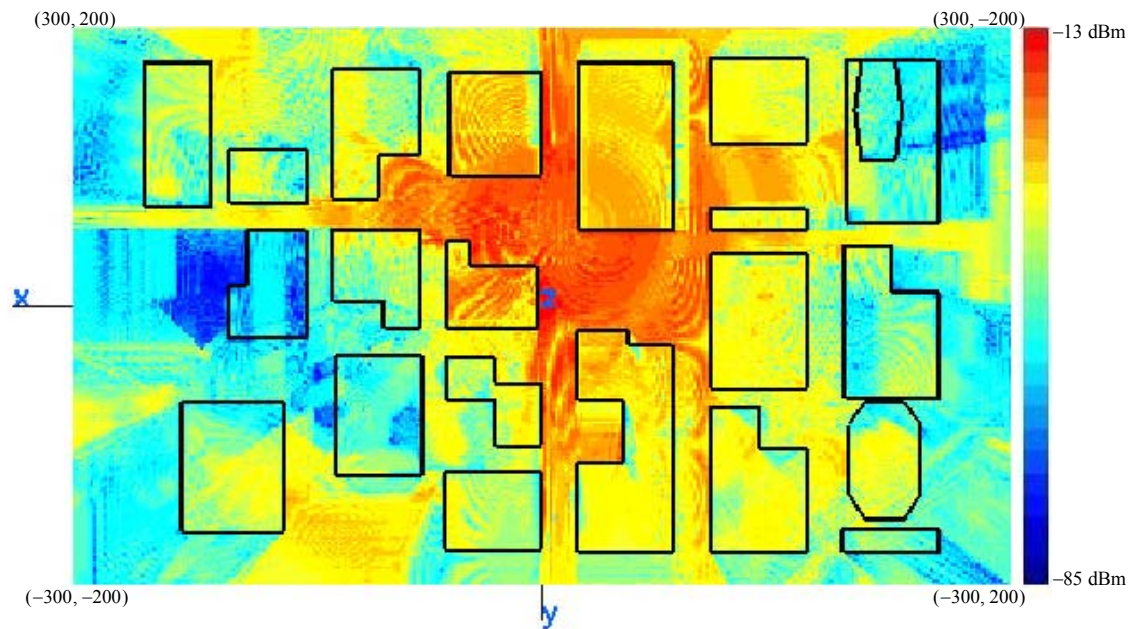

Figure 37.   Signal coverage for two horizontal transmit dipoles at locations
$(-10 \text{ m}, -55 \text{ m}, 150 \text{ m})$ and $(-10.167 \text{ m}, -55 \text{ m}, 150 \text{ m})$

Figures 38 and 39 show the comparison of the received signal power when using spatial diversity on transmit for vertical and horizontal cases, respectively. The two curves, shown for each case, are for diversity on receive (red plot) and no receive diver-

sity (blue plot). The signal powers for the receive diversity are computed assuming EGC technique at the receivers. The performances for both cases are similar to that of having no transmitter diversity as discussed in the following paragraph.
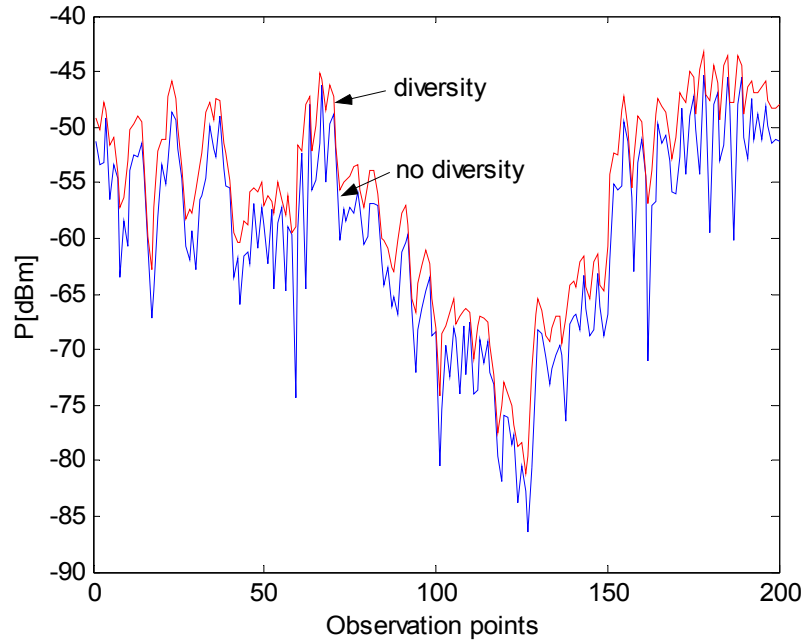
Figure 38. Spatial diversity on transmit, vertical case: comparison of diversity on receive vs. no diversity
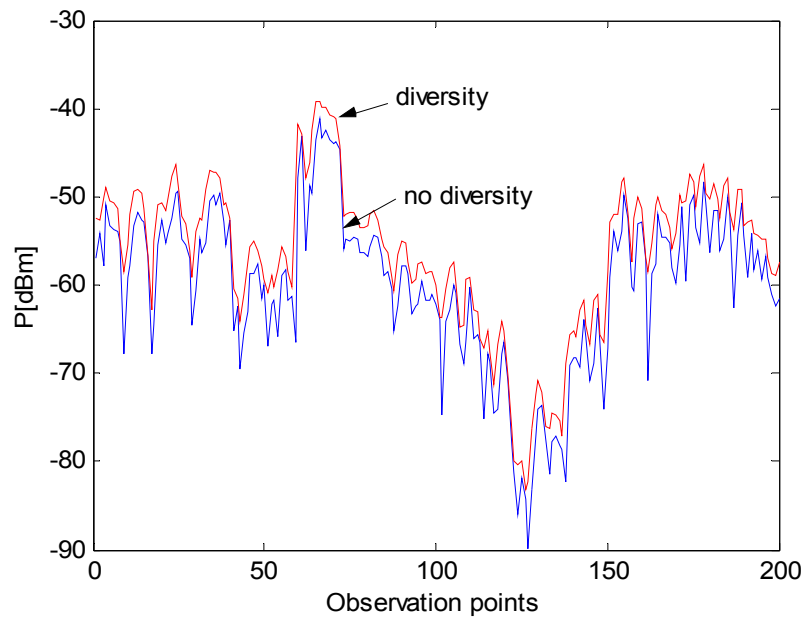
Figure 39. Spatial diversity on transmit, horizontal case: comparison of diversity on receive vs. no diversity

Figures 40 and 41 show a comparison of diversity on transmit (red plot) and no transmit diversity (blue plot) for vertical and horizontal cases, respectively. It is observed that transmit diversity has only slight improvement over the no diversity case. As explained in Chapter III previously, spatial diversity on transmit has its primary advantage in MIMO where high spectral efficiency can be achieved.
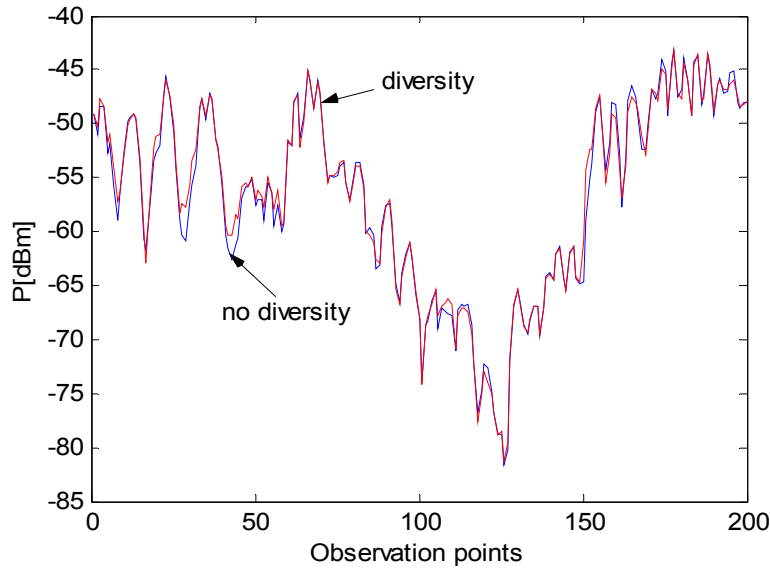
Figure 40.   Spatial diversity on receive, vertical case: comparison between diversity on transmit and no diversity
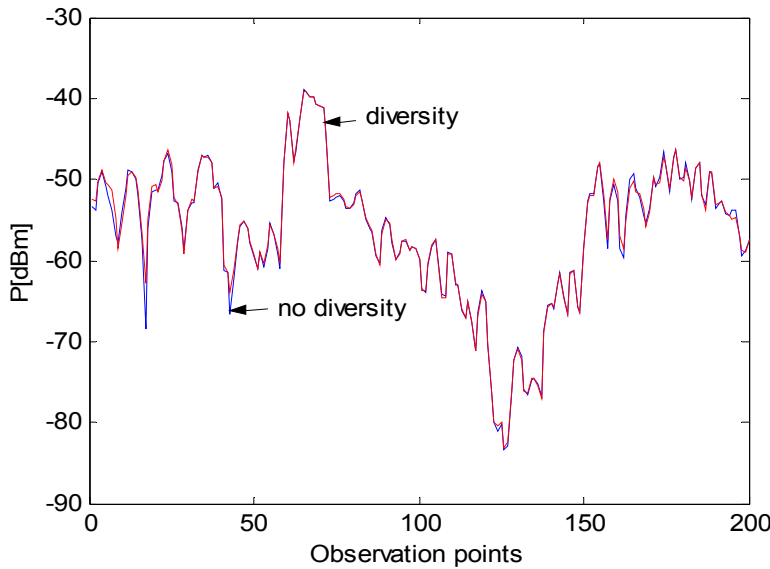
Figure 41.   Spatial diversity on receive, horizontal case: comparison between diversity on transmit and no diversity

B.   SIMULATIONS OF POLARIZATION DIVERSITY

Antenna dual-polarization diversity was simulated with two orthogonally polarized co-located $\lambda/2$ dipoles, with one orientated horizontally, the other vertically. This method is advantageous when area is limited on the platform and spatially dispersed antennas cannot be installed. A few scenarios using various antenna configurations on both transmit and receive were investigated.

1.   Polarization Diversity on Transmit with Horizontal Dipole on Receive

In this scenario, the UAV transmitter antenna was modeled as two orthogonally polarized $\lambda/2$ dipoles. Each dipole was excited by a zero-phase half unit power. The receiver antenna is a single horizontally polarized $\lambda/2$ dipole. Table 6 shows the parameters used in the simulation.

PARAMETERS	SETTINGS
Operating Frequency	900 MHz
Type of Tx antenna	2 dipoles
Length of Tx antenna	0.1667 m
Locations of Tx antenna	$(-10$ m, -55 m, 150 m) and $(-10$ m, -55 m, 150 m)
Tx power/phasing	$0.5\angle 0°$ W and $0.5\angle 0°$ W
Orientations of Tx antenna	parallel to the z axis and parallel to the y axis
Observation points (used for signal coverage plot computation)	600 m by 400 m with cell size of 2 m, height of 1.5 m
Type of Rx antenna	dipole
Length of Rx antenna	0.1667 m
Locations of Rx antenna	$(145$ m, 200 m, 1.5 m) to $(145$ m, -200 m, 1.5 m) with 2 m resolution
Orientation of Rx antenna	parallel to the y axis

Table 6.   Urbana input parameters for simulation of dual-polarization diversity on transmit with horizontal dipole on receive

The total signal strength plot is shown in Figure 42. It is observed that strong signals are concentric around the transmitter location. The strongest received signal strength is about -16 dBm while the weakest is -81 dBm.
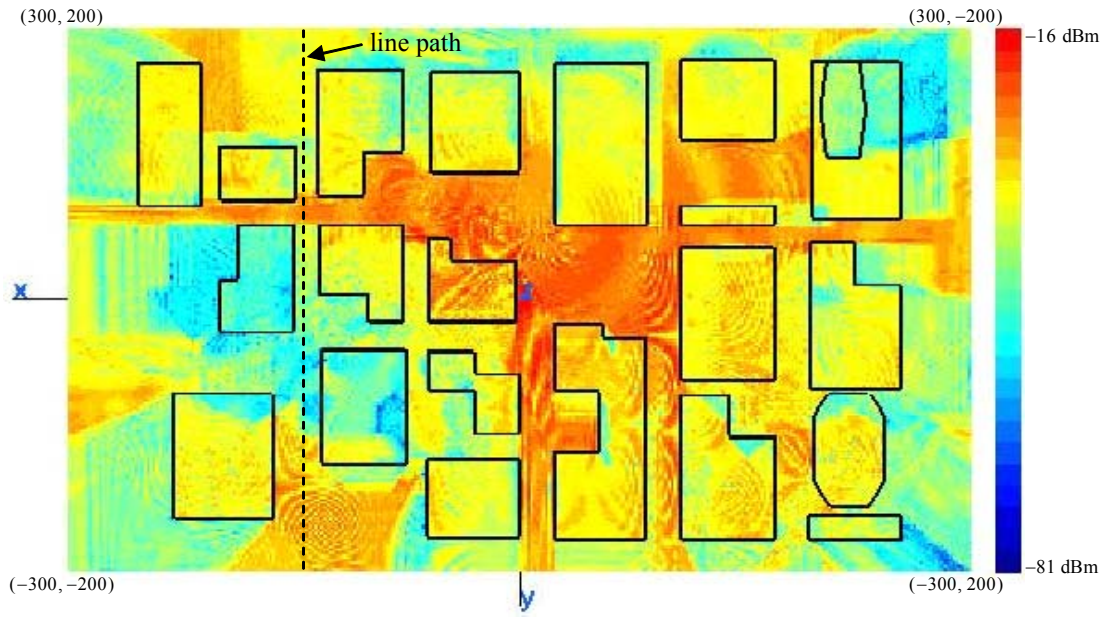
Figure 42.   Signal coverage plot for dual-polarized transmit dipoles at location $(-10 \text{ m}, -55 \text{ m}, 150 \text{ m})$

For further analysis, a horizontal dipole on receive was simulated over the line path of 200 observation points. Figure 43 shows the received signal strength on the line path from (145 m, 200 m, 1.5 m) to (145 m, −200 m, 1.5 m) at 2 m increments.
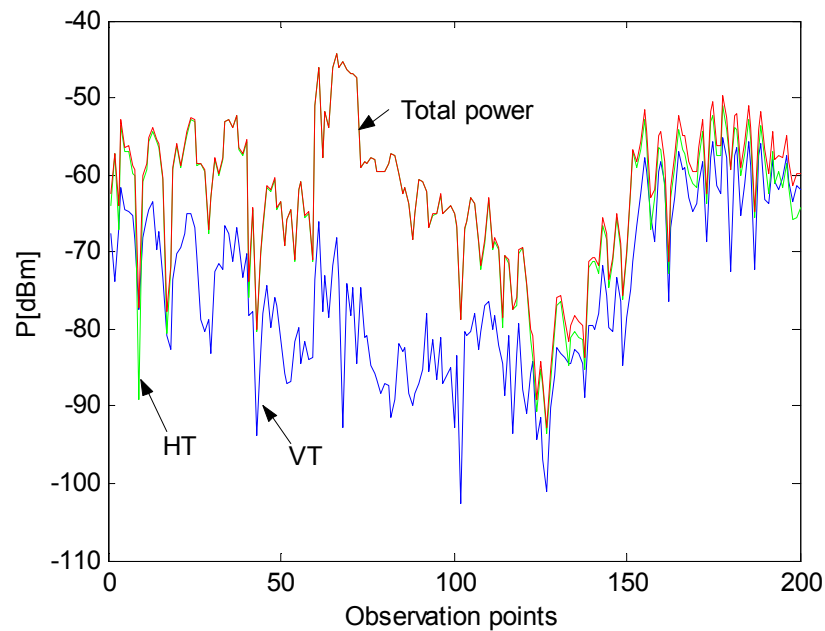
Figure 43.   Dual-polarized transmit antenna with a horizontal dipole on receive

The received total power is contributed by both the vertical element (VT) and horizontal element (HT) of the dual-polarized transmitter antenna. It is observed that the main contribution to the total signal strength is from the horizontally polarized element of the dual-polarized transmitter antenna. This is expected as the receivers are horizontally polarized antennas.

2. Polarization Diversity on Transmit with Vertical Dipole on Receive

In this scenario, the receiver antennas were configured to be vertically polarized $\lambda/2$ dipoles. Table 7 shows the parameters used in the simulation.

PARAMETERS	SETTINGS
Operating Frequency	900 MHz
Type of Tx antenna	2 dipoles
Length of Tx antenna	0.1667 m
Locations of Tx antenna	$(-10$ m$, -55$ m$, 150$ m$)$ and $(-10$ m$, -55$ m$, 150$ m$)$
Tx power/phasing	$0.5\angle 0°$ W and $0.5\angle 0°$ W
Orientations of Tx antenna	parallel to the z axis and parallel to the y axis
Type of Rx antenna	dipole
Length of Rx antenna	0.1667 m
Locations of Rx antenna	$(145$ m$, 200$ m$, 1.5$ m$)$ to $(145$ m$, -200$ m$, 1.5$ m$)$ with 2 m resolution
Orientation of Rx antenna	parallel to the y axis

Table 7.   Urbana input parameters for simulation of dual-polarization diversity on transmit and a vertical dipole on receive

Vertical receiving dipoles were simulated over the line path from (145 m, 200 m, 1.5 m) to (145 m, -200 m, 1.5 m) at 2 m increments. The results are shown in Figure 44. The received total power is contributed by both the vertical (VT) and horizontal (HT) elements of the dual-polarized transmitter antenna. The main contribution to the total signal strength is from the vertically polarized element (VT) of the dual-polarized transmitter antenna. This is expected because the receivers are vertically polarized dipoles.
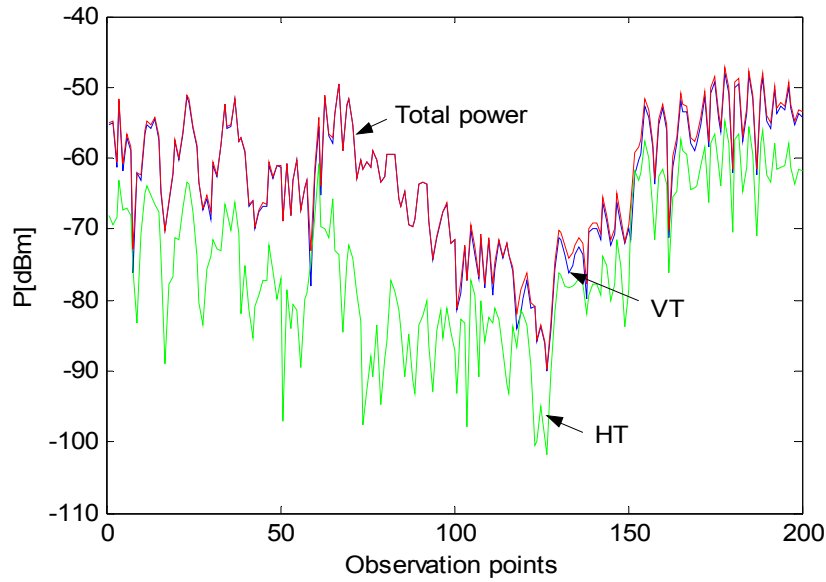
Figure 44.   Dual-polarized transmit antenna with a vertical dipole on receive

3.   Polarization Diversity on both Transmit and Receive

In this scenario, dual-polarization diversity was simulated for both the transmitter and receiver antennas. The dual-polarized receiver dipoles were simulated over the line path. Table 8 shows the parameters used.

PARAMETERS	SETTINGS
Operating Frequency	900 MHz
Type of Tx antenna	2 dipoles
Length of Tx antenna	0.1667 m
Locations of Tx antenna	(−10 m, −55 m, 150 m) and
	(−10 m, −55 m, 150 m)
Tx power/phasing	0.5∠0° W and 0.5∠0° W
Orientations of Tx antenna	parallel to the z axis and
	parallel to the y axis
Type of Rx antenna	2 dipoles
Length of Rx antenna	0.1667 m
Locations of Rx antenna	(145 m, 200 m, 1.5 m) to (145 m, −200 m, 1.5 m)
	with 2 m resolution
Orientations of Rx antenna	parallel to the z axis and
	parallel to the y axis

Table 8.   Urbana input parameters for simulation of dual-polarization on transmit and receive

51

The results of this simulation were combined with the results of the previous scenarios. A comparative analysis was done to assess the performance of various combinations of polarization diversity. These are discussed in the following paragraphs.

Figure 45 compares between dual-polarized, vertical, and horizontal dipoles on receive, with the transmitter on dual-polarized dipoles. EGC technique was assumed to be implemented at the receivers. It is observed that a horizontal dipole on receive (HT) has the advantage over a vertical dipole (VT) at observation points near to the transmitter location (50 to 125). However, for dual-polarized dipoles on receive (DPR), the received signal power is improved relative to a single polarization. For example, at the deep fading location, the dual-polarized receiver has about a 5-dB signal strength advantage over the horizontally polarized receiver. However, it is to be noted that the SNR improvement would be 2 dB as noise power is doubled (3 dB) in EGC.
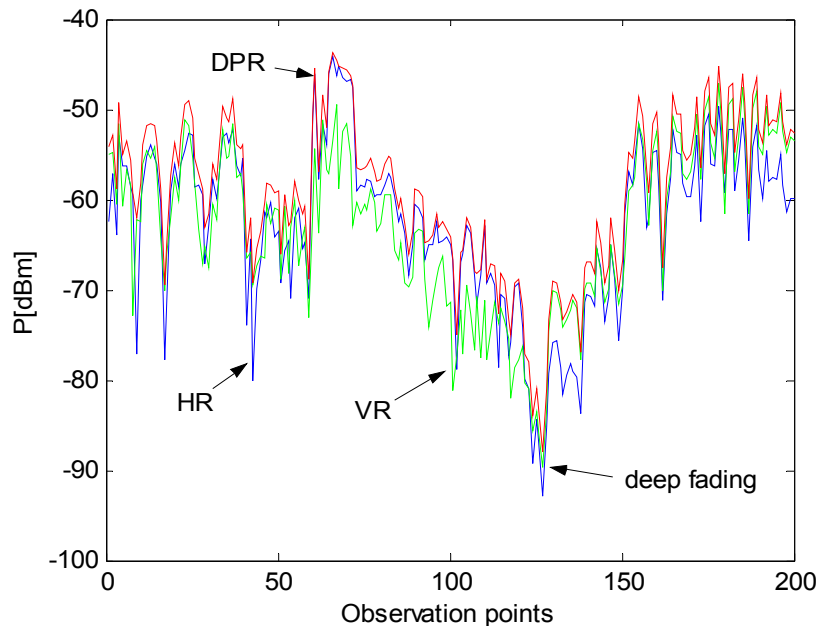
Figure 45.   Dual-polarization diversity on transmit: comparison between dual-polarized, vertical, and horizontal dipoles, on receive

In Figure 46, the case of dual-polarized dipoles on transmit and receive (DPTR) is compared to a vertical dipole on transmit and receive (VTR), and a vertical dipole on transmit and dual-polarized dipoles on receive (VTDPR). The plot shows that the dual-polarized dipoles on transmit and receive (red plot) has better received signal power at

most locations. However, at the deep fading location, there is no advantage of the dual-polarized dipoles on transmit over the other two configurations. In addition, at observation points (125 to 200), it has a number of drastic drops of signal strength (fading).
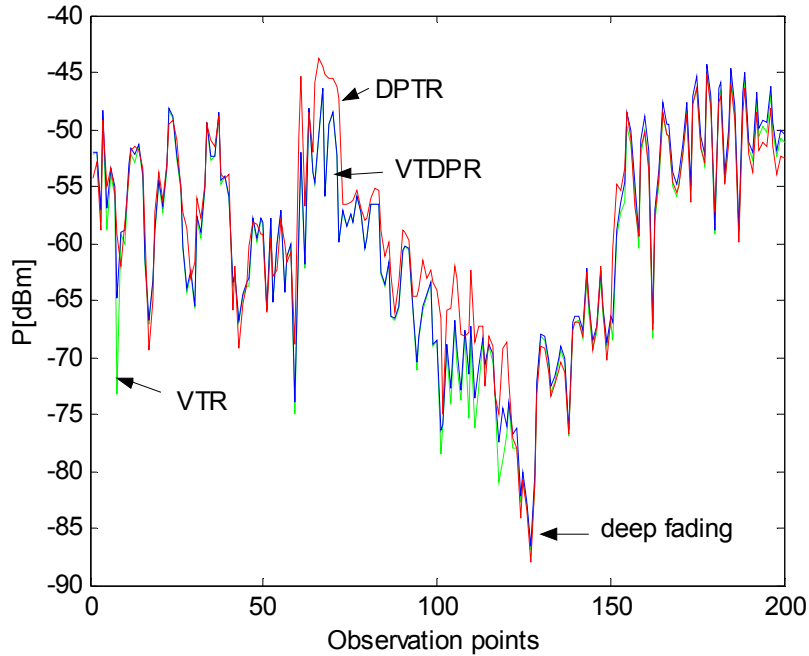
Figure 46.   Comparison between dual-polarized and vertical dipole on transmit and receive

Figure 47 compares the case where dual-polarized dipoles on transmit and receive (DPTR), against horizontally (DPTHDR) and vertically (DPTVDR) polarized spatial diversity on receive. At the deep fading location, the vertical case has a slight improved signal power of about 3 dB as compared to dual-polarized diversity on receive. The horizontally polarized spatial diversity gives improved signal strength at observation points near to the transmitter (50 to 125). For dual-polarization on transmit, it is obvious that spatial diversity on receive has an advantage over dual-polarization on receive.
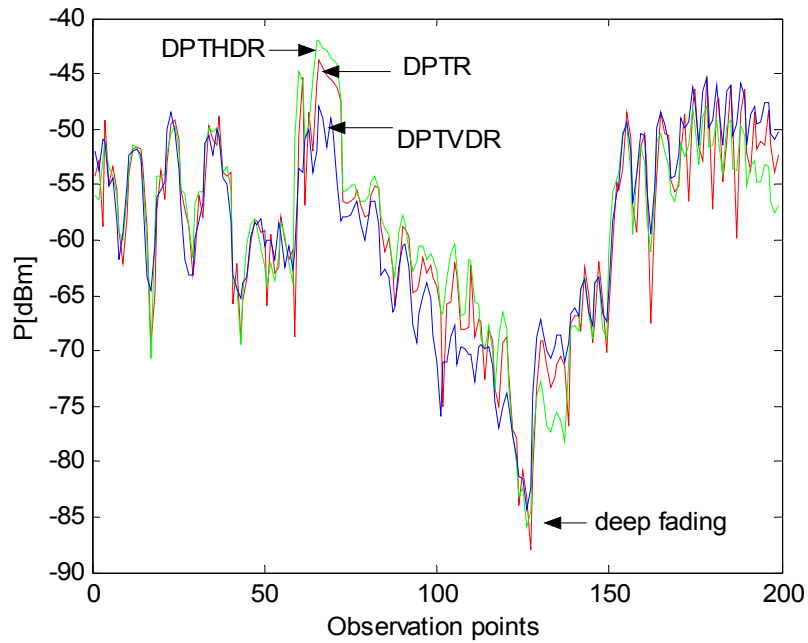
Figure 47.   Dual-polarization diversity on transmit: comparison between dual-
polarized dipoles and spatial diversity on receive

Finally, a comparison was done for spatial diversity and polarization diversity on both transmit and receive. In Figure 48, the spatial diversity (red plot) performs better than the dual-polarization diversity (blue plot). For example, at the deep fading point, the spatial diversity technique gives about 7 dB improvement. At observation points near to the transmitter (50 to 125), both give comparable signal strengths. In addition, the numbers of drastic signal drops (fading) have reduced significantly for the spatial diversity as compared to the polarization diversity case.
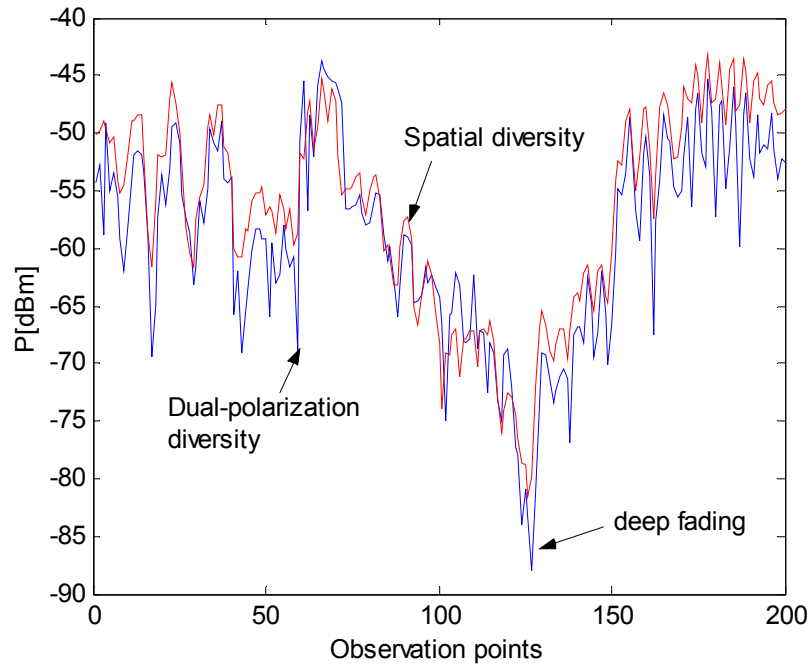
Figure 48.   Comparison between dual-polarization diversity and spatial diversity on both transmit and receive

C.   SIMULATIONS OF ANGLE DIVERSITY

In the simulation of angle diversity, a directional antenna was modeled at the receiver while a $\lambda/2$ dipole was modeled on the transmitting UAV. The characteristic of the directional antenna was discussed in Chapter IV. The radiation patterns are shown in Figures 24 and 25. In order to investigate the effects of angle diversity, the transmitter locations were taken at discrete points along a flight path.

1.   Angle Diversity on Receive

Table 9 shows the parameters used for simulation of a single dipole on transmit with angle diversity on receive. There are five transmitter locations. The location of the receiver is chosen to be at (145 m, 52 m, 1.5 m). This location was chosen from the line path of observation points that were used in the previous diversity analyses. The purpose was to assess the performance of angle diversity over the other techniques, which did very little to mitigate the deep fading.

55

PARAMETERS	SETTINGS
Operating Frequency	900 MHz
Type of Tx antenna	dipole
Length of Tx antenna	0.1667 m
Locations of Tx antenna	Tx #1 at $(-80 \text{ m}, 45 \text{ m}, 150 \text{ m})$
	Tx #2 at $(-45 \text{ m}, -5 \text{ m}, 150 \text{ m})$
	Tx #3 at $(-10 \text{ m}, -55 \text{ m}, 150 \text{ m})$
	Tx #4 at $(25 \text{ m}, -105 \text{ m}, 150 \text{ m})$
	Tx #5 at $(60 \text{ m}, -155 \text{ m}, 150 \text{ m})$
Tx power/phasing	$1\angle 0° \text{ W}$
Orientation of Tx antenna	parallel to the z axis
Observation points (used for signal coverage plot computation)	600 m by 400 m by 1.5 m with 2 m resolution
Type of Rx antenna	directional (See Figure 24)
Location of Rx antenna	(145 m, 52 m, 1.5 m)
Orientation of Rx antenna	variable (depending on direction of strongest incoming signals)

Table 9.   Urbana input parameters for simulation of angle diversity on receive

Figure 49 shows the five waypoints of the flight path of a transmitting UAV. The waypoints are the locations where transmission is simulated. The signal strength coverage plots of a $\lambda/2$ dipole transmitting at location Tx #1 to Tx #5 are shown in Appendix D.

In investigating the performance of angle diversity, the receiver location (Rx) at (145 m, 52 m, 1.5 m) uses the directional antenna pointed towards the strongest incoming signal ray for each transmitting location. The location Tx #3 was the same transmitter location as for the other diversity techniques, and therefore this point was used to compare performance with the other diversity techniques. The data for the rest of the transmitting locations are shown in Appendix D.
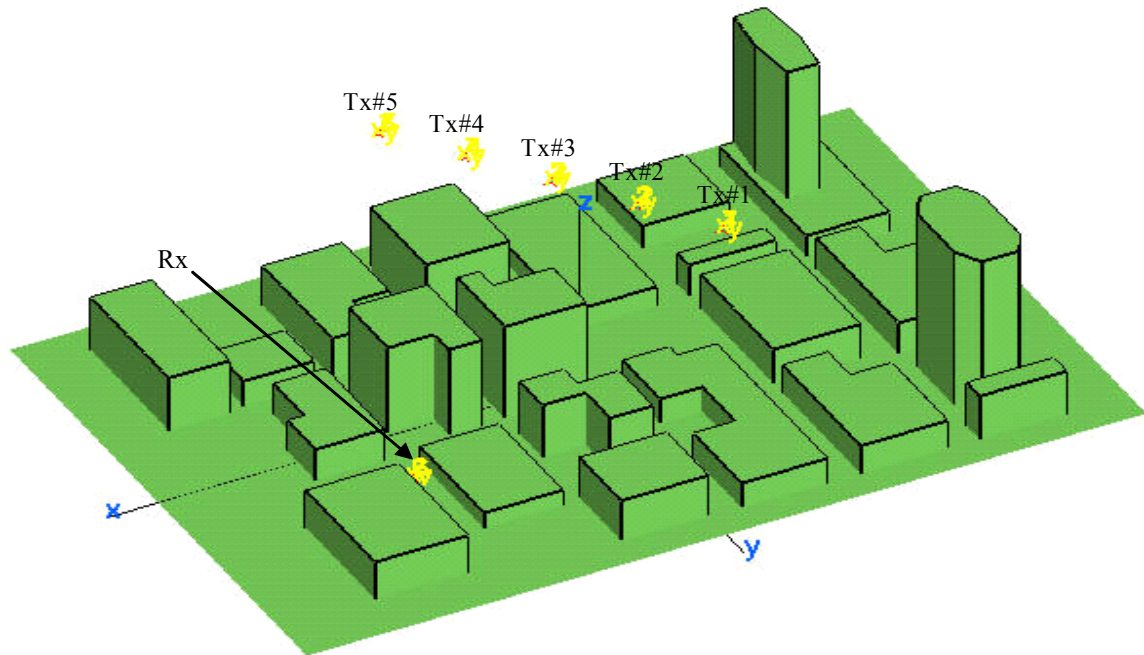
Figure 49.   Transmit locations for the UAV flying across the city

Figure 50 shows the angle-of-arrival (AOA) data for a dipole receiver at location (145 m, 52 m, 1.5 m) with the dipole transmitter at Tx #3. The vectors in Figure 50(a) point to the directions of the arriving rays at the receiver. Figure 50(b) gives the power level of each arriving ray, while Figures 50(c) and 50(d) give the angles ϕ and θ of each ray. Appendix B shows the representation of angles ϕ and θ in the coordinate system used in Urbana. From these four figures, it can be deduced that the strongest signal is Ray Number #15, and it has an AOA of $\phi = 45°$ and $\theta = -38°$.
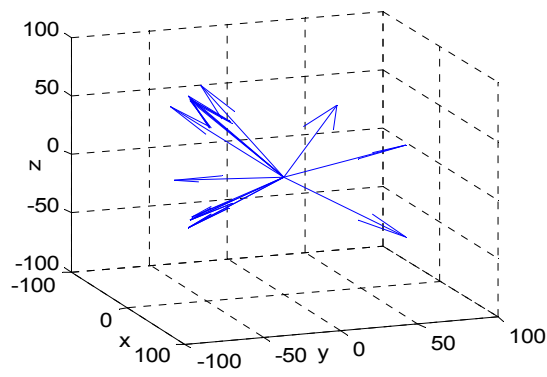
(a) Ray AOAs (b) Ray power levels
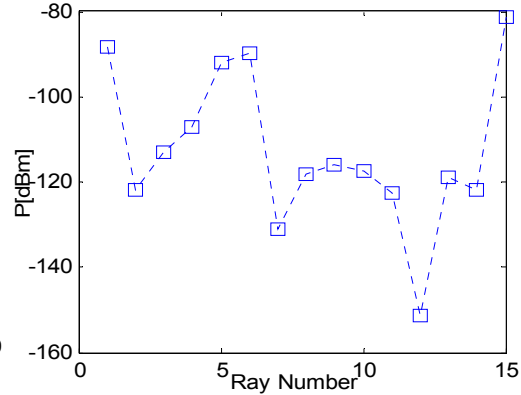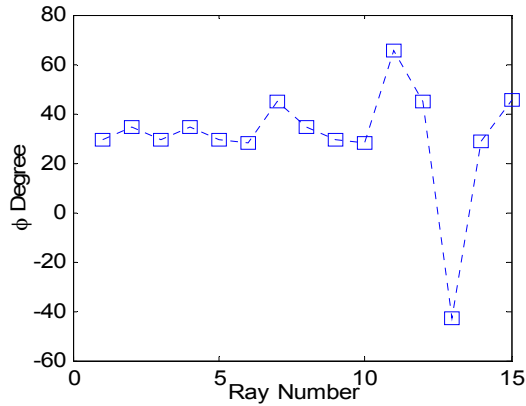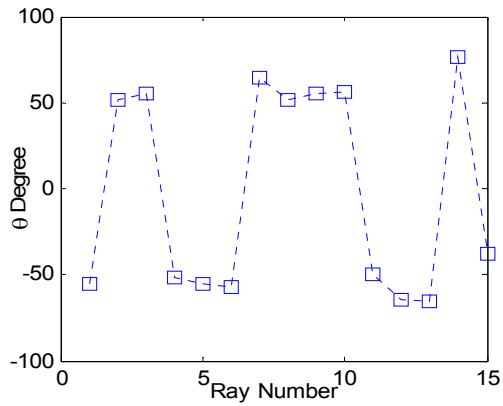
(c) Angle ϕ of rays (d) Angle θ of rays

Figure 50.   Signal rays received by dipole receiver at location (145 m, 52 m, 1.5 m)
when transmitting from Tx #3

With the AOA data, the directional antenna was set to point towards the direction
of the highest power ray. The simulated results are shown in Figure 51. By comparing
with Figures 50(a) and 51(a), it is observed that with the directional antenna, there are
fewer numbers of arriving rays at the receiver as compared to the dipole receiver. This is
primarily due to the fact that the antenna radiation pattern in its rear hemisphere is zero.
This is good for rejecting interference coming from the rear direction, thus a good signal-
to-interference ratio. Looking at Figures 50(b) and 51(b), it is also observed that there is
improvement in the received signal power for the directional antenna receiver.

| (a) Rays AOAs | (b) Ray power levels |
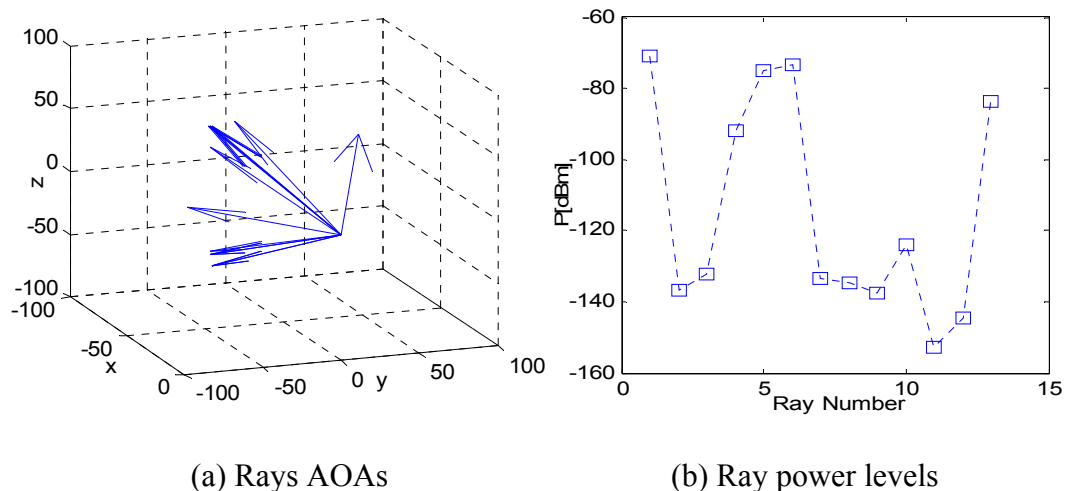
Figure 51.   Signal rays received by directional antenna at location (145 m, 52 m, 1.5 m) when transmitting from Tx #3

In a more detailed analysis, Urbana aggregates the signal strength of each arriving ray and computes the total received power and outputs the result to a *couple* file. Table 10 compares the total received power at location (145 m, 52 m, 1.5 m) for the dipole and directional antenna receiver for transmit positions Tx #1 to Tx #5. It is noted that at the deep fading location of (145 m, 52 m, 1.5 m), a directional antenna employing angle diversity would be able to provide a significant improvement in the received signal power (from 11 dB to 23 dB).

Transmitter	Received Power		Antenna Direction (ϕ,θ)	Received Power Improvement
	Dipole	**Directional Antenna**		
Tx #1	−63.68 dBm	−51.65 dBm	(2°, −55°)	12.03 dB
Tx #2	−66.88 dBm	−55.61 dBm	(17°, −52°)	11.27 dB
Tx #3	−86.96 dBm	−63.27 dBm	(45°, −38°)	23.69 dB
Tx #4	−69.14 dBm	−48.91 dBm	(52°, −53°)	20.23 dB
Tx #5	−67.01 dBm	−47.00 dBm	(68°, −56°)	20.01 dB

Table 10.   Total received power for a dipole and directional antenna receiver

D.   SUMMARY OF FINDINGS

This chapter presented various simulations implementing the techniques of (1) spatial diversity, (2) polarization diversity, and (3) angle diversity, for UAV urban data links.

Table 11 shows a comparison of the received signal power at receive location (145 m, 52 m, 1.5 m) and transmitting location Tx #3 for each diversity technique that was investigated in this thesis. It is obvious that angle diversity has the best performance as compared to the rest, while spatial diversity with two dipoles also has shown a significant increase.

Receiver at deep fading location (145 m, 52 m, 1.5 m)	Transmitter at location Tx #3	Received Signal Strength
One vertical dipole (No diversity)	One vertical dipole	−86.96 dBm
Two vertical dipoles (Spatial diversity)	Two vertical dipoles	−81.19 dBm
Two horizontal dipoles (Spatial diversity)	Two horizontal dipoles	−83.19 dBm
Dual-polarized dipoles (Polarization diversity)	Dual-polarized dipoles	−87.98 dBm
Two vertical dipoles (Spatial diversity)	Dual-polarized dipoles	−82.35 dBm
Two horizontal dipoles (Spatial diversity)	Dual-polarized dipoles	−84.44 dBm
Directional antenna (Angle diversity)	One vertical dipole	−63.27 dBm

Table 11.   Comparison of performance for different diversity techniques

For spatial diversity, it was demonstrated that diversity on receive can improve the received signal strength. For example, with two vertical receive dipoles there is an improvement of about 6 dB at the location of deep fading (145 m, 52 m, 1.5 m), compared to the case where no diversity is used. The SNR improvement is 3 dB with EGC at the receivers. Spatial diversity with vertical dipoles has shown better performance over spatial diversity with horizontal dipoles. The vertical case has a smaller number of significant signals fades as compared to the horizontal case. The exception is if the receivers are located below the transmitter. Then horizontal dipoles would provide better performance. Further improvement may be possible using more than two antennas on receive, but this comes at the expense of increased size and complexity.

With regard to space limitation, polarization diversity is a good option to consider. A few combinations of polarization and spatial diversity were computed for comparison. Polarization diversity on transmit and spatial diversity on receive has shown the best performance of all the combinations. For example, with dual-polarized dipoles on transmit and spatial diversity on receive, there is a signal strength improvements of about 2.5 dB and 4.5 dB for horizontal and vertical dipoles on receive, respectively. With EGC at the receivers, the SNR improvements are -0.5 dB and 1.5 dB, respectively. This is for the location of deep fading and relative to the no diversity case. The overall performance is also not as good as the spatial diversity technique.

For angle diversity, the results have shown that it has much higher received signal strength relative to both the spatial and polarization diversity techniques. For example, when compared to spatial diversity on both receive and transmit (vertical cases), at transmitting location of Tx #3, the signal strength at the deep fading location improved by about 23 dB. When angle diversity is compared with polarization diversity on both receive and transmit, the improved received signal strength is about 25 dB. In addition, the angle diversity provides for good signal-to-interference ratio at the receiver. However, the disadvantage of angle diversity is that the receiver would need to be equipped with the capability (i.e., an adaptive antenna) to detect the direction of the strongest arriving signal rays and then to turn the antenna beam in that direction.

THIS PAGE INTENTIONALLY LEFT BLANK

VI.   CONCLUSIONS AND FUTURE WORK

A.   CONCLUSIONS

The urban environment complicates military communications. The challenge for MOUT is to achieve effective tactical communications in locations where radiowave propagation is subjected to multipath and fading because of buildings and other structures obstructing the signals. UAVs and diversity techniques, however, can be used to mitigate these effects and improve the reliability of communications.

In this thesis, three diversity techniques were investigated to assess their performance in an urban environment. They were (1) spatial diversity, (2) polarization diversity, and (3) angle diversity. These techniques were simulated for a UAV platform operating over a small city model. The findings can be summarized as follows. Angle diversity has shown the most significant improvement in received signal strength as compared to the other two techniques, but the implementation of such directional antennas would be complex. Spatial diversity on receive has shown better overall improvement as compared to polarization diversity. Further improvement is possible with more spatially uncorrelated antennas, but its implementation could be limited by the availability of space. Polarization diversity on transmit and receive has shown good received signal strength only at some locations over the spatial diversity technique. However, a combination of polarization diversity on transmit and spatial diversity on receive has better overall performance. An advantage of polarization diversity is that the two orthogonal linear polarizations can usually be obtained with a single antenna. This is especially appealing for UAV applications, where space on the platform is limited.

This research has demonstrated the potential of implementing diversity techniques for improving UAV data links in MOUT. It should be noted that the simulation performed did not cover all possible system and environment parameters. A limited number of transmitter-receiver geometries were examined. However, care was taken to select cases that included direct LOS (strong signals) and non-LOS shadows (faded signals). This allows a comparison of various techniques under a range of conditions, so that some general conclusions could be reached.

B. FUTURE WORK

1. Full Spectrum Modeling and Simulation

A detailed profiling of an exact operational urban area, e.g., downtown Baghdad, would be useful. For example, details like lamp posts, trees and roads can be modeled and simulated to examine their impact on the diversity techniques. A range of frequencies relating to different types of UAV systems can also be simulated. This would provide for a full spectrum comparison of the diversity techniques, to include frequency diversity.

2. Verification and Validation of Models

With detailed profiling and modeling, it would be possible to compare the model with measured real-world data. For example, a 900-MHz VTOL UAV system using spatial diversity on receive can be prototyped for testing in an actual environment to verify and validate the results of the simulation. This would provide a feedback on the model's accuracy and reliability, and thus enhancements to the model, if required.

3. Linkages to Operation Research Models

There is a possibility of integrating the modeling and simulation results in Urbana to the existing C4SIR operation models from Air Force Agency for Modeling and Simulation (AFAMS), and Army Model and Simulation Office (AMSO). The idea is to explore integration of the findings into the existing operational models for more insightful pursuit.

4. Investigation of Channel Coherence Bandwidth and Coherence Time

Further study of the urban radiowave propagation channel can be extended to analyze its channel coherence bandwidth and time characteristics. For example, Urbana can be used to compute the RMS delay spread of the received signals, which can be used to compute the coherence bandwidth and coherence time of the channel.

The coherence time information, which defines the "static-ness" of the channel, is useful when considering the Doppler effects due to motions of transmitter, receiver, and surrounding objects. Coherence bandwidth information gives the maximum frequency

difference of the signals that are still strongly correlated in amplitude. This limits the signal bandwidth [15].

5   SDMA and Smart Antenna Modeling

For further simulation of angle diversity or SDMA for urban UAV data links, adaptive antenna receivers can be modeled. An adaptive antenna would dynamically adjust its radiation pattern to minimize the effects of noise, interference, and mutipath [18]. The use of an adaptive array to maximize SNR would result in suppression of noise jamming signals. Using an adaptive algorithm, e.g., the least-mean-square (LMS) algorithm, simulations can be run to analyze the performance.

6   Simulation of Jamming

The effectiveness of the diversity techniques against communications jamming can be simulated. For example, a transmitting jammer antenna can be simulated at a certain location, and then the received jamming signals at various receiving locations can be computed. Together with the no jamming received signals, the jamming-to-signal ratio (JSR) can be calculated. With the various diversity techniques simulated at the receivers, different JSR can be computed and compared.

THIS PAGE INTENTIONALLY LEFT BLANK

APPENDIX A.   URBANA CODES

The following are listings of typical Urbana user input file and reprocessing input file of *filename.ur_input* and *filename.urrp_input*, respectively:

```
--- input Urbana v 2.5
#
# ********************************
# A---scatterer file,length & freq
# ********************************
#--- name of scatterer file in ACAD format (e.g. wall.facet)
citywgrnd.facet
#--- length unit:1=inch, 2=cm, 3=meter, 4=mm, 5=mil
3
#--- uniform freq (GHz): start freq, end , nstep
#    (nstep=0 means: just do first freq. CAUTION: antenna patterns are
#     assumed to be indep. of freq and is calculated at end freq)
0.9 0.9 0
#
# ********************************
# B--- Antenna Description and List
# ********************************
#
#---Enter method of describing antennas.
#   (1 = here, 2 = file):
1
#---If described in file, enter file name:
city.antenna
#---If described here, fill in sections B1, B2, B3.
#   If described in file, use dummy data in sections B1, B2, B3
#   (specify one dummy antenna type, dummy antenna origin,
#    and one dummy item in antenna list).
#
# *********************
# B1: Define Antenna Types
# *********************
#
#   Two lines for each type.
#     Line1: type ID, ant code
#     Line2: parameters
#
#   Type ID must start from 1 and increment by 1 thereafter
#
#   Ant Code   meaning              parameters
#   --------   ----------------     ----------------------------
#      1       pattern file         filename(ascii)
#      2       dipole               length(real)
#
```

```
#    Antenna Types list:
#
#    Enter number of antenna types:
1
#    Type #1
1 2
0.1667
#
# ***********************************************
# B2: Enter origin of antenna coord in main coord
# ***********************************************
#
0.  0.  0.
#
# **********************
# B3: Create Antenna List
# **********************
#
#    Three lines for each antenna.
#      Line1: Type ID, location (x,y,z), power (watts), phase(deg)
#      Line2: Local x-axis in main coord.
#      Line3: Local z-axis in main coord.
#
#    Enter number of antennas:
1
#
#    Antenna #1
1  -10 -55 150 1. 0.
1. 0. 0.
0. 0. 1.
#
# **********************
# C---Observation points
# **********************
#--- Observation points defined with respect to main coord. system 7.
#    Enter method of specifying list of points.
#    (1 = here, 2 = file):
2
#--- If points are listed here, enter number of points (kobtot):
1
#--- If listed here (1 above), List xyz of points in main coord 7
#    (one point at a line). If 2 above, include one dummy line.
1.           2.              -11.00
#--- If points listed in file (2 above), enter name of file.
observ15.obv
#--- Include direct Tx to observer contribution.
#    If you turn on the direct contribution from the transmitter to the
#    observation point, computed result will be the total field, which
is
#    the incident + scattered field.   For propagation analysis, this
is
#    the preferred setting.  Otherwise, the result only includes the
#    scattered field.
#
```

```
#     Include direct contribution from transmitter to observation point
(rx)
#     (1 = yes, 0,2 = no):
1
#--- Compute received power into Rx antenna.
#     Urbana always computes field levels at the observation point.
#     If you specify an Rx antenna, Urbana will also compute the re-
ceived
#     power and record the results in the (runname).couple file.
#     This causes a moderate but slow-down when using the SBR method
(below).
#
#     Include Rx antenna (1 = yes, 0,2 = no):
1
#--- Rx antenna specification
#     Remaining entries in Section C can be ignored if not including
#     an Rx antenna.
#     Enter antenna type (1 = pattern file, 2 = dipole):
2
#     Each antenna type requires additional parameters.
#     List of expected parameters follows.  Choose one.
#
#     Type  Description     Expected Parameter(s)
#     1     Pattern File    File Name (e.g., beam.antpat)
#     2     Dipole          Length (in prevailing unit)
#
#     Enter parameter(s) on next line:
0.1667
#--- Rx antenna orientation
#     Enter local x-axis of Rx in global coordinates
1. 0. 0.
#     Enter local z-axis of Rx in global coordinates
0. 0. 1.
#
# ****************************
# D---Theoretical consideration
# ****************************
#--- Choose method of computation
#     0 = compute fields in the ABSENCE of the scatterer
#     1 = compute fields by SBR
#     2 = compute fields by GO
2
#--- If SBR, select a PO integration scheme at bounce points
#     1 = do integration at first & last bounce points only
#     2 = do so at all bounce points (GTD formulation)
1
#--- Edge diffraction
#     SBR can be enhanced with PTD edge diffraction.
#     GO can be enhanced with GTD edge diffraction.
#     Add edge diffraction (0,2=no, 1=ILDC (SBR or GO), 3=UTD (GO only)
3
#--- If edge diffraction switched on, enter name of edge file
#     (e.g., wall.edge or dummy if edge not included).
city.edge
```

```
#--- Choose method of ray launch
#    1 = by (baby) facet, achieving a uniform first bounce surface den-
sity
#    2 = uniform angular distribution (burst launch)
#    (If computation by GO, must select 2 = burst launch)
2
#--- If ray launch by (baby) facet (1 above), enter ray density:
#    # rays/wavelength (normally 5-10)
5.
#--- If burst ray launch (2 above), enter angular interval (deg).
#    (Typically 0.25 - 2.0 deg)
2.
#--- max permissible ray bounces (normally 5-10)
7
#--- max-voxdepth = max depth of BSP tree (normally 20)
#    max-voxl = max facets in each voxel(normally 10)
#    (Larger voxdepth & smaller voxl lead to faster ray-tracing
#     but more computer memory)
20,10
#--- ICOAT for absorbing facets
888
#--- IQMATRIX for divergence factor
#     1 = calculated by Q-matrix
#     2 = ignored except for the spherical wave spread
2
#--- IF using Q-matrix, name target curvature file(e.g. wall.curv)
dummy.curv
#--- IPEC=1 if all pec,  =2 if coating present
2
#--- For PEC scatterer, give the magnitude of reflection coeff
#    (use 1.0 for ideal PEC, use less for rough PEC--fudging)
1.0
#--- IF PEC, the rest coating info is dummmy
#--- material reflection is done through a look-up table
#    specify the freq interval in GHz for the table e.g. 0.25
#    (dummy if input freq less than 51)
0.2
********************
E---coating material
********************
---- number of materials
     (NOT including pec, which is identified by ICOAT=0)
     (NOT including absorbing facets:  ICOAT=28 or 888)
     (If 3 material, urbana reads only ICOAT=1-3)
3  <----NCOTOT
--- for each material, identify its boundary type:
    iboundary = 1 if impedance boundary
                2 if layered slabs with PEC backing
                3 if penetrable layered slabs with air backing
                4 if penetrable FSS Tx/Refl table supplied by user
                5 if same as 2 except using freq-dep ramlib.d
                6 if antenna refl table supplied by user
                7 if layers over semi-infinite ground
for each material, given info by following the templates
```

```
^^^ ICOAT=1 ^^^^^^^^^^^^^^^^^^^^^^^^^^^^^^^^^^^^^^^^^^^^^^^^^^^^^^^
--- iboundary
3
--- number of layers over air backing
    (1st layer is farthst fr incid field and innermost)
1
--- thick,epsilon(c),mu(c),resistivity(ohm)
0.30000 (10.1,0.5) (1.0,0.0) 1.e+30
^^^ ICOAT=2 ^^^^^^^^^^^^^^^^^^^^^^^^^^^^^^^^^^^^^^^^^^^^^^^^^^^^^^^
--- iboundary
2
--- number of layers over PEC backing
    (1st layer is farthst fr incid field and innermost)
2
--- thick,epsilon(c),mu(c),resistivity(ohm)
0.0300 (2.5,-0.000) (1.6,-0.000) 1.e+30
0.0500 (3.0,-0.000) (1.0,-0.000) 1.e+30
^^^ ICOAT=3 ^^^^^^^^^^^^^^^^^^^^^^^^^^^^^^^^^^^^^^^^^^^^^^^^^^^^^^^
--- iboundary
7
--- number of layers over half-space (semi-infinite ground)
    (1st layer is farthst fr incid field and innermost)
1
--- thick,epsilon(c),mu(c),resistivity(ohm)
0.1000 (3.000,-0.0) (1.0,-0.0) 1.e+30
--- epsilon(c),mu(c) of semi-infinite ground
(3.00,-0.00) (1.0,-0.00)

(End of regular input file. Leave a few blank lines)

------------------------------------------------------------------
'OPTIONAL ADVANCE FEATURES' (Do not change letters in quotations)
# The line above must be placed at the end of the regular urbana
# input. Advance features are designed for special applications or
# for testing codes.  They are not needed by general usages.
# ------------------------------------
# ADVANCE1: ADD GTD-TYPE BLOCKAGE CHECK
# ------------------------------------
# In regular urbana computation, blockage check is mostly done by
# PTD principle. For interior scattering in a confined region, use of
# GTD principle may be more appropriate.
# Option to use GTD principle:  1=yes,    2=no (regular case)
2
# ----------------------------------------
# ADVANCE2: SIMPLE TERRAIN BLOCKAGE MODEL
# ----------------------------------------
# For GO method, terrain generates 100% blockage, and blocked rays
leave
# no energy behind a hill.  With this feature, LOS rays and UTD edge
# diffraction rays can pass through terrain, with some attenuation.
# Attenuation is measured in dB per hill.  Each hill is identified
# by two passages through two terrain facets.
# Can only be used with GO method (and UTD edge option).
# Use simple terrain model: 1 = yes, 2 = no (regular case)
2
# Enter coating code range of terrain facets (e.g., 1, 2):
1 1
```

71

```
# Enter amount of attenuation per hill (dB, > 0):
5.
# -------------------------------------------------
# ADVANCE3: APPROXIMATE DOUBLE DIFFRACTION MODEL
# -------------------------------------------------
# For GO + UTD method, only single diffraction is considered.
# With this feature, double diffraction is approximated by identifying
# surfaces which block the single diffraction, such as building walls.
# If one or two facets block the path from the single diffraction point
# to the transmitter, the diffraction is still included, but with at-
tenuation.
# Works best if "diffracting facets", marked by their coating code, are
# always associated with enclosed structures with well defined edges.
# Use double diffraction model: 1 = yes, 2 = no (regular case)
2
# Encounter coating code range of diffracting facets (e.g., 5, 10):
2 2
# Enter amount of attenuation for second diffraction (dB, > 0);
10.
# ----------------------
# ADVANCE4: ACCELERATION
# ----------------------
# For large scenes, run time grows both with the number of field
# observation points and the number of edges.  Normally, all combina-
tions
# of lit edges and observation points are considered.  This feature
# accelerates the processing by limiting the scope of considered edge
# interactions to region around the LOS path from the transmitter
# to the observation point.  For example, to run a 5 km by 5 km scene,
# one may choose a 250 m interaction radius.  For each observation
# point, edges are ignored that lie outside an ellipse whose foci are
the
# Tx and the observation point and whose major axis is the LOS distance
# plus 500 m (radius x 2).
# This feature can also be used to automatically filter edge files
# whose domain far exceeds the domain of observation points.
# Only use this feature for terrestrial simulations where the scene
# is nominally parallel to the x-y plane.
#
# Use large scene acceleration: 1 = yes, 2 = no (regular case)
2
# Enter radius of interaction
250.
# --------------------------
# ADVANCE5: MULTI-DIFFRACTION
# --------------------------
# Substitute for Adv. #3.  Uses ray rubber-banding algorithm to find
# path from transmitter to receiver.
# Can only be used with GO. Cannot be used in conjunction with Adv. #3.
# If UTD switched on above, will take measures not to double count
# single diffraction mechanisms.
# Use multi-diffraction model: 1 = yes, 0,2 = no
2
# Enter coating code range of diffracting facets (e.g. 5, 10):
2 2
```

```
# Enter maximum number of rubber-band points ( also used in Advance6 )
1
# Check multiple crawl planes instead of just vertical one: 1 = yes,
0,2 = no
0
# -------------------------
# ADVANCE6: REFLECTION-DIFFRACTION
# -------------------------
# If UTD switched on above, will take measures not to double count
# single diffraction mechanisms.
# Use reflection-diffraction model: 1 = yes, 0,2 = no
2
# Do more than just single diffractions: 1 = yes, 0,2 = no
# Allow rubber-banding to both transmitter and receiver: 1 = yes, 0,2 =
no
1 0
# Choose crawl plane selection mode: 0 = always vertical, 1 = initial
edge,
#                                    2 = adaptive from edge to edge
1
# ------------------------------------
# ADVANCE7: GREEN'S FUNCTION (GF) FILE
# ------------------------------------
# By default, for SBR and no-target methods, a GF file IS NOT produced.
# Also, by default, for GO, a GF file IS produced.
# Use this feature to explicitily activate or de-activate generation
# of the GF file, which is needed by the re-processor for its activi-
ties.
# Activate GF file: 0 = no, 1 = yes, 2 = default activation behavior
0
# If yes, enter buffer scale factor.  Increasing scale factor reduces
# the number of GF file dumps to disk during a run, but costs memory.
# Recommend 2 - 5 for GO method, 1 for no-target method,
# and 100 - 10000 for SBR method.
2


--- input Urbana_rp v 1.2
#
# *******************************
# A---scatterer file,length & freq
# *******************************
#--- name of scatterer file in ACAD format (e.g. wall.facet)
citywgrnd.facet
#--- length unit:1=inch, 2=cm, 3=meter, 4=mm, 5=mil
3
#--- uniform freq (GHz): start freq, end , nstep
#    (nstep=0 means: just do first freq. CAUTION: antenna patterns are
#     assumed to be indep. of freq and is calculated at end freq)
0.9 0.9 0
#
# *******************************
# B--- Antenna Description and List
# *******************************
#
```

```
#---Enter method of describing antennas.
#   (1 = here, 2 = file):
1
#---If described in file, enter file name:
cityant.antenna
#---If described here, fill in sections B1, B2, B3.
#   If described in file, use dummy data in sections B1, B2, B3
#   (specify one dummy antenna type, dummy antenna origin,
#    and one dummy item in antenna list).
#
# ***********************
# B1: Define Antenna Types
# ***********************
#
#   Two lines for each type.
#      Line1: type ID, ant code
#      Line2: parameters
#
#   Type ID must start from 1 and increment by 1 thereafter
#
#   Ant Code    meaning            parameters
#   --------    ---------------    ----------------------------
#     1         pattern file       filename(ascii)
#     2         dipole             length(real)
#
#   Antenna Types list:
#
#   Enter number of antenna types:
1
#   Type #1
1 2
0.1667
#
# ***********************************************
# B2: Enter origin of antenna coord in main coord
# ***********************************************
#
0. 0. 0.
#
# ***********************
# B3: Create Antenna List
# ***********************
#
#   Three lines for each antenna.
#      Line1: Type ID, location (x,y,z), power (watts), phase(deg)
#      Line2: Local x-axis in main coord.
#      Line3: Local z-axis in main coord.
#
#   Enter number of antennas:
1
#
#   Antenna #1
1  -10 -55 150 1. 0.
1. 0. 0.
0. 0. 1.
#
```

```
# *************************
# C---Greens' function files
# *************************
1
omnirxdiv.gf
#
# *********************
# D---Reprocessor Output
# *********************
#
# Generate field data (1 = yes, 0 = no)?
1
# Generate angle of arrival data (1 = yes, 0 = no)?
1
#--- Compute received power into Rx antenna.
#    Urbana_rp will record the results in the (runname).couple file.
#    If angle of arrival data are also being generated, will also
#    record the received signal per contribution in that file.
#
#    Include Rx antenna (1 = yes, 0,2 = no):
1
#--- Rx antenna specification
#    Remaining entries in this section can be ignored if not including
#    an Rx antenna.
#    Enter antenna type (1 = pattern file, 2 = dipole):
2
#    Each antenna type requires additional parameters.
#    List of expected parameters follows.  Choose one.
#
#    Type  Description     Expected Parameter(s)
#    1     Pattern File    File Name (e.g., beam.antpat)
#    2     Dipole          Length (in prevailing unit)
#
#    Enter parameter(s) on next line:
0.1667
#--- Rx antenna orientation
#    Enter local x-axis of Rx in global coordinates
1. 0. 0.
#    Enter local z-axis of Rx in global coordinates
0. 0. 1.
```

THIS PAGE INTENTIONALLY LEFT BLANK

APPENDIX B.   COORDINATE SYSTEM

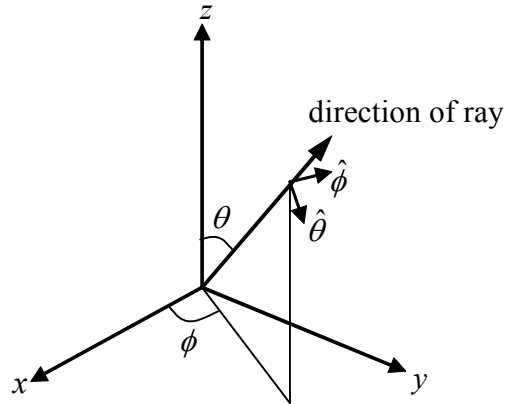The coordinates system used in Urbana is shown in Figure 52.

Figure 52.   Urbana coordinates system

THIS PAGE INTENTIONALLY LEFT BLANK

APPENDIX C.   MATLAB CODES

The Matlab codes used to generate the observation points and antenna pattern file are shown below. Also, included are the codes for computing the received power for two dipoles diversity on transmit with two dipoles diversity on receive, and no diversity on receive. Similar programs were written for other combinations of diversity, but are not included here. A sample program for computing the AOA data at the fixed receiving location for one of the transmitting location are also shown.

A.   Generate Observation Points

```
% Observation Points Generation
clc;
clear;

step = 2; %footprint of 2 m
i = 1;
z = 1.5; %height of 1.5 m

for x = -300:step:300
    for y = -200:step:200
        M(i,:)=[x,y,z];
        i=i+1;
    end
  end

lines=i-1
save observ.obv M -ASCII;
```

B.   Generate Antenna Pattern File

```
% Antenna Pattern File Generation
clc;
clear;

lamda = (3*10^8)/(900*10^6);
HPBW = 10; % in degrees
a = 58.4 * lamda / (2*HPBW) % Uniform Circular Aperature Size (radius)
beta = 2*pi/lamda;
E0 = 1;
c = j*beta*E0*pi*a^2/(2*pi); %Contant term in E field
```

```matlab
Directivity = (4*pi*pi*a^2)/lamda^2
Directivity_dB = 10*log10(Directivity)

step1 = 90; %Vertical Steps
step2 = 180; %Horizontal Steps
d_theta = 180/(step1);
d_phi = 360/(step2);
k = 0;
ip = 0;
iq = 0;

   for phi = 0:d_phi:360
     for theta = -90:d_theta:90 %plots out the zero point
        k = k+1;
        arg=beta*a*sin(theta*pi/180);
        f = 1;
        if abs(arg)>=1e-5
         f = 2*besselj(1,arg)/arg;
        end
        e_theta = cos(phi*pi/180)*c*f;
        e_phi = -sin(phi*pi/180)*cos(theta*pi/180)*c*f;
        if theta > 90
           e_theta = 0;
           e_phi = 0;
        end
        if phi == 0
           ip = ip + 1;
           et0(ip) = 20*log10(abs(e_theta));
           ep0(ip) = 20*log10(abs(e_phi));
           eth(ip) = theta;
        end
        if phi == 90
           iq = iq + 1;
           et90(iq) = 20*log10(abs(e_theta));
           ep90(iq) = 20*log10(abs(e_phi));
           eth90(iq) = theta;
        end
        A(k,1:4) = [real(e_theta), imag(e_theta), real(e_phi), imag(e_phi)];
     end
   end

   save antennapat -ASCII;

   figure(1)
   plot(eth,et0,eth,ep0)
   title('Directional Antenna Pattern (HPBW=10 degrees)')
```
80

```
xlabel('Angle [degree]')
ylabel('Relative Power [dB]')
figure(2)
plot(eth90,et90,eth90,ep90)
xlabel('Angle [degree]')
ylabel('Relative Pattern, dB')
```

C.   Computation of Received Power Data

```
%Received Power for Diversity on transmit and receive
clc;
clear;
Txantdiv=2;
TF=0;

fid=fopen('city2antx.couple','r');  % 2 dipoles transmit diversity couple file
line0=fgetl(fid);  % to rid of the header
while TF==0
   line1=fgetl(fid);
   obv=sscanf(line1,'%i %*i %*f %*f %*f');
   antid=sscanf(line1,'%*i %i %*f %*f %*f');  % antenna id
   powerdBm(obv,antid)=sscanf(line1,'%*i %*i %*f %f %*f'); % power value
   TF=feof(fid);
end
fclose(fid);

for n=1:obv-1  %coherently adding at two observation points
   powerdiv1(n)=(10^((powerdBm(n,1))/10))+(10^((powerdBm(n+1,1))/10));
   powerdiv2(n)=(10^((powerdBm(n,2))/10))+(10^((powerdBm(n+1,2))/10));
   powerdiv1Bm(n)=10*log10(powerdiv1(n));   % power from Tx1 to 2 Rx div
   powerdiv2Bm(n)=10*log10(powerdiv2(n));  % power from Tx2 to 2 Rx div
   powerdivtot(n)=powerdiv1(n)+powerdiv2(n); % coherent addition of 2 Rx
   powerdivtotdBm(n)=10*log10(powerdivtot(n));
   powertot(n)=(10^((powerdBm(n,1))/10))+(10^((powerdBm(n,2))/10));
   powertotdBm(n)=10*log10(powertot(n));  % power from Tx1 & Tx2 to 1 Rx (no div)
end

n=1:obv-1;
hold on
plot(powertotdBm(n),'b')  % 2 Tx and no Rx div
plot(powerdivtotdBm(n),'r') % 2 Tx and Rx div
xlabel('Observation points')
ylabel('P[dBm]')
hold off
```

D.   Computation of AOA Data

```
% AOA Data Generation for one receiving location
clc;
clear;
n=0;
cnt=0;
TF=0;

fid=fopen('omni900M_Tx1.aor','r');

while TF==0
   line0=fgetl(fid);
   f=sscanf(line0,'%*s %*s %i%*s %*s %*s %i');

   for n = 1:f(2)   %no of rays
      line1=fgetl(fid);
      line2=fgetl(fid);
      line3=fgetl(fid);
      antid=sscanf(line1,'%i %*i %*i %*f %*f %*f %*f %*f');
      r=sscanf(line3,'(%f,%*f)');
      im=sscanf(line3,'(%*f,%f)');
      raypoweri=(r^2 + im^2); %for testing of valid ray only
      if (raypoweri > 0)
         cnt=cnt+1;
         type(f(1),antid,cnt)=sscanf(line1,'%*i %i %*i %*f %*f %*f %*f %*f'); %ray type

         bounce(f(1),antid,cnt)=sscanf(line1,'%*i %*i %i %*f %*f %*f %*f %*f'); %no.
         of bounces of ray

         x(f(1),antid,cnt)=sscanf(line1,'%*i %*i %*i %*f %*f %f');
         y(f(1),antid,cnt)=sscanf(line1,'%*i %*i %*i %*f %*f %*f %f');
         z(f(1),antid,cnt)=sscanf(line1,'%*i %*i %*i %*f %*f %*f %*f %f');

         ph=atan(y(f(1),antid,cnt)/x(f(1),antid,cnt));

         phi(f(1),antid,cnt)=rad2deg(ph);
         %phi_angle for one observation point, tx antenna, ray

         theta(f(1),antid,cnt)=rad2deg(atan(y(f(1),antid,cnt)/(z(f(1),antid,cnt)*sin(ph))));
         % theta_angle for one observation point, tx antenna, ray

         raypowerf(f(1),antid,cnt)=raypoweri; %actual ray power
      end
   end
   ray(f(1))=cnt; %no of actual rays for the fixed receiving point
   cnt=0;
```

```
    TF=feof(fid);
end

fclose(fid);

figure(1)
q=1:ray(f(1)); %get the exact no of rays for the fixed receiving point
p=phi(f(1),1,q);
clear s;
s(q)=p;
plot(q,s,':s')
title('AOA from Tx#')
xlabel('Ray Number')
ylabel('\phi Degree')

figure(2)
t=theta(f(1),1,q);
clear u;
u(q)=t;
plot(q,u,':s')
title('AOA from Tx#')
xlabel('Ray #')
ylabel('\theta Degree')

figure(3)
rp=10*log10((raypowerf(f(1),1,q))*1000);
clear w;
w(q)=rp;
plot(q,w,':s')
title('Power of rays from Tx#')
xlabel('Ray #')
ylabel('P[dBm]')

figure(5)
gx=gradient(x(f(1),1,q));
gy=gradient(y(f(1),1,q));
gz=gradient(z(f(1),1,q));
quiver3(gx,gy,gz,x(f(1),1,q),y(f(1),1,q),z(f(1),1,q),100) %plot the aor of rays
view([70 18])
title('Direction of rays from Tx#')
xlabel('x')
ylabel('y')
zlabel('z')
```

THIS PAGE INTENTIONALLY LEFT BLANK

APPENDIX D.   SIGNAL COVERAGE AND RAYS PLOTS FOR ANGLE DIVERSITY

The signal coverage and rays plots for Tx #1 to Tx #5 are shown below.

A.   Signal Coverage Plots for Tx #1 to Tx #5
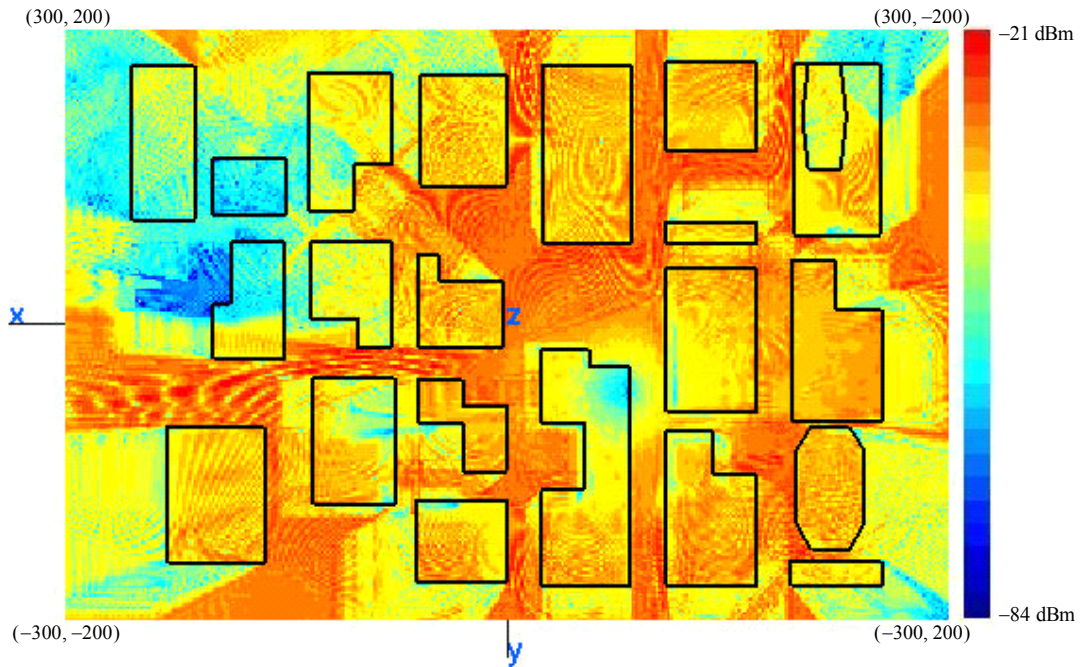
Figure 53.   Signal coverage for Tx #1

(300, 200)　　　　　　　　　　　　　　　　　　(300, −200)

−21 dBm

−80 dBm

(−300, −200)　　　　　　　　　　　　　　　　　(−300, 200)

Figure 54.　　Signal coverage for Tx #2

(300, 200)　　　　　　　　　　　　　　　　　　(300, −200)

−21 dBm

−82 dBm

(−300, −200)　　　　　　　　　　　　　　　　　(−300, 200)
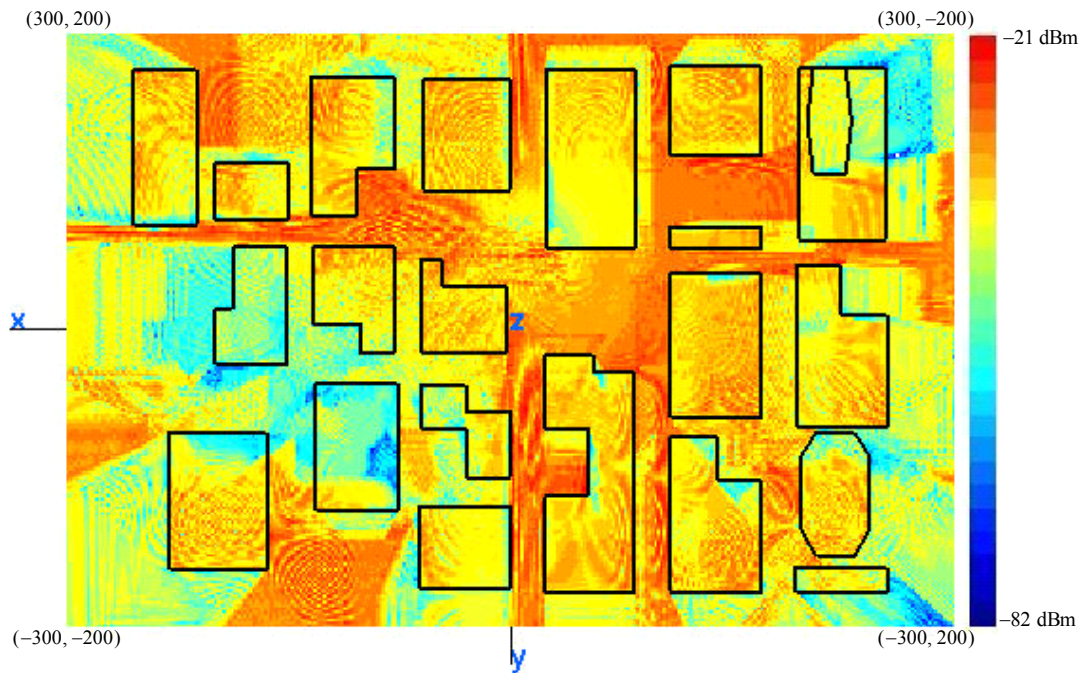
Figure 55.　　Signal coverage for Tx #3

(300, 200)   (300, −200)
                                                                            −20 dBm

x ———   z

                                                                            −77 dBm
(−300, −200)   y   (−300, 200)
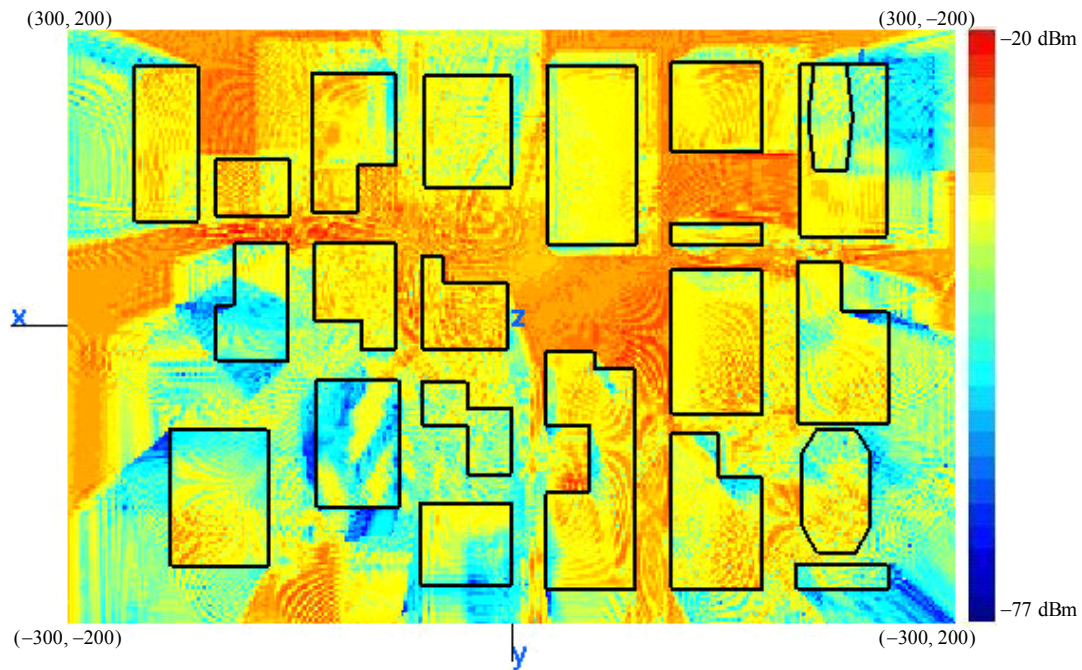
Figure 56.   Signal coverage for Tx #4

(300, 200)   (300, −200)
                                                                            −21 dBm

x ———   z

                                                                            −83 dBm
(−300, −200)   y   (−300, 200)
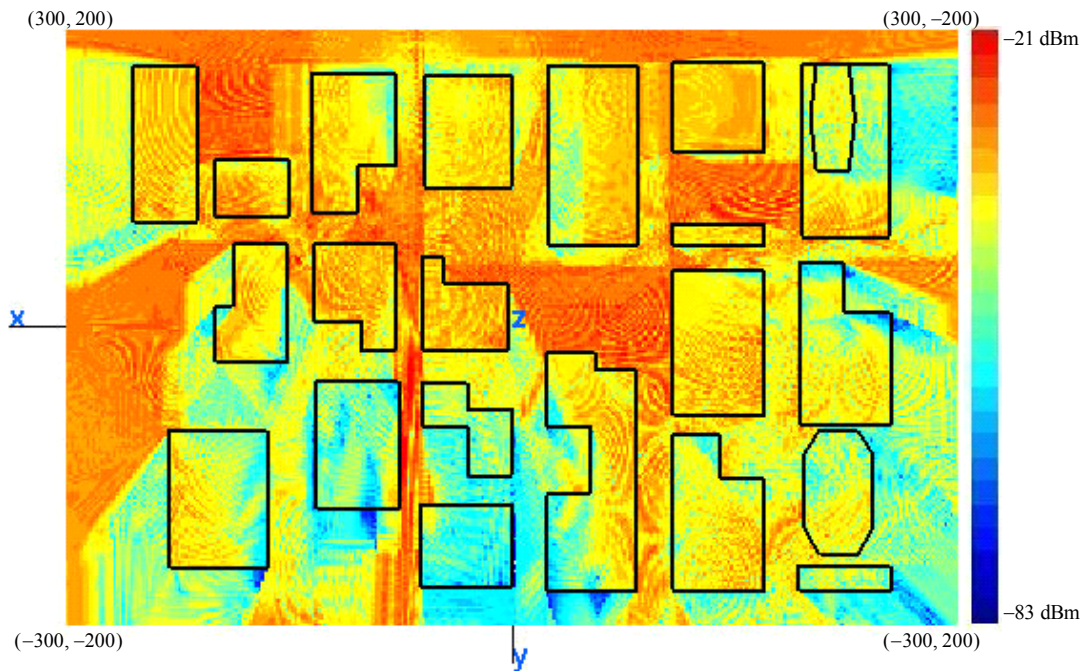
Figure 57.   Signal coverage for Tx #5

87

B.   Signal Rays Plots for Tx #1
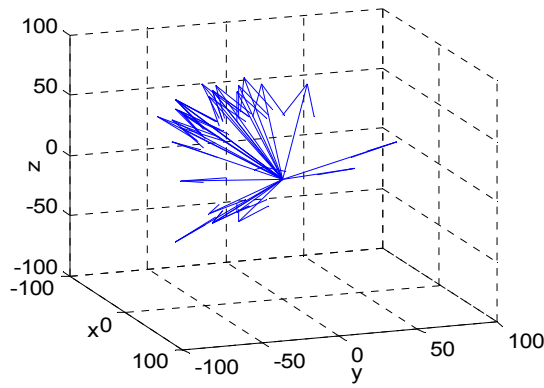
(a) Ray AOAs
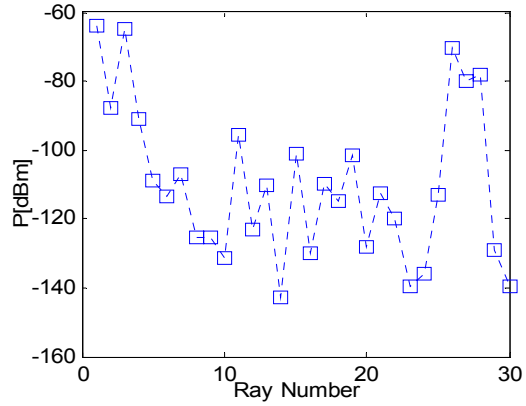
(b) Ray power levels
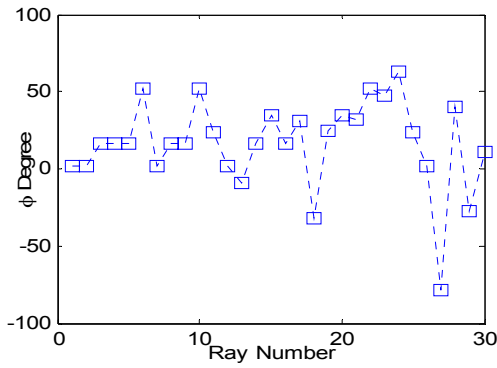
(c) Angle ϕ of rays
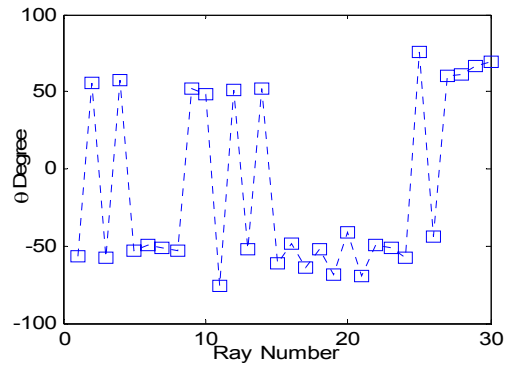
(d) Angle θ of rays

Figure 58.   Signal rays received by dipole receiver at location (145 m, 52 m, 1.5 m) when transmitting from Tx #1
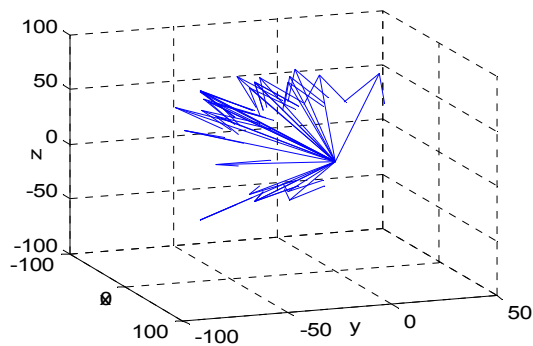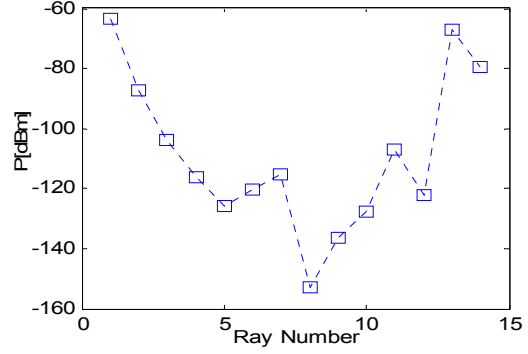

(a) Ray AOAs plot
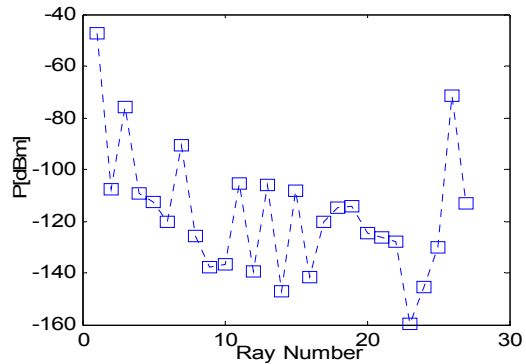
(b) Ray power levels

Figure 59.   Signal rays received by directional antenna at location (145 m, 52 m, 1.5 m) when transmitting from Tx #1
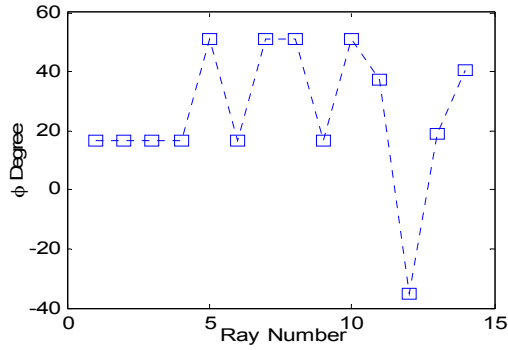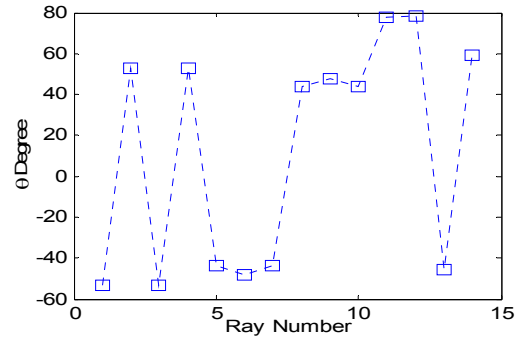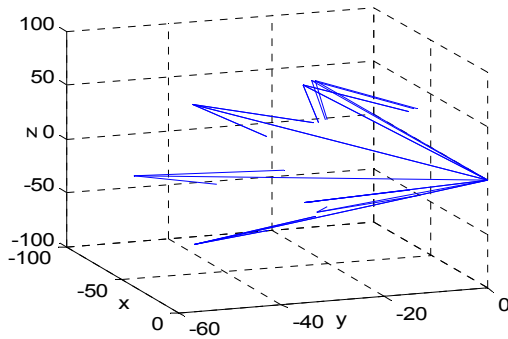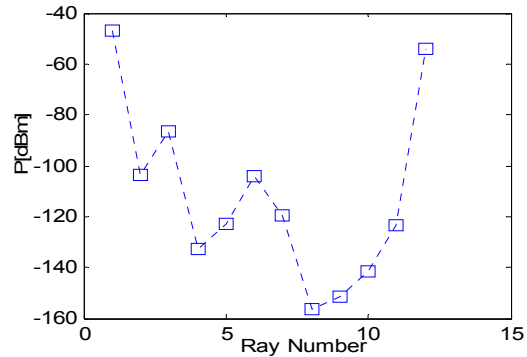
C.   Signal Rays Plots for Tx #2
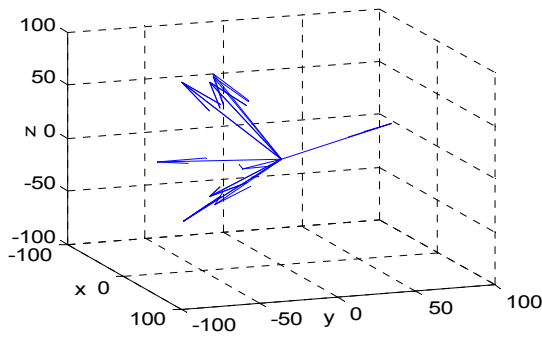
(a) Rays AOAs

(b) Ray power levels

(c) Angle ϕ of rays

(d) Angle θ of rays

Figure 60.   Signal rays received by dipole receiver at location (145 m, 52 m, 1.5 m) when transmitting from Tx #2

(a) Rays plot

(b) Power level of rays

Figure 61.   Signal rays received by directional antenna at location (145 m, 52 m, 1.5 m) when transmitting from Tx #2
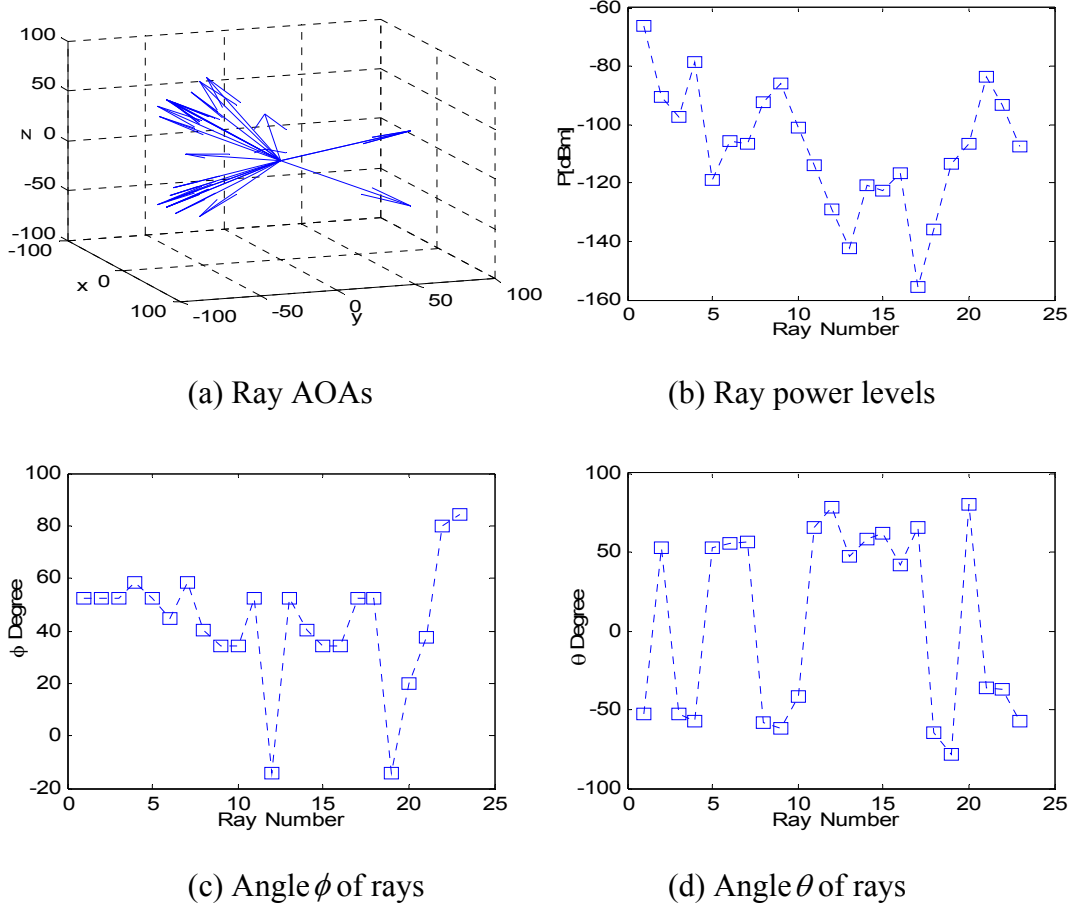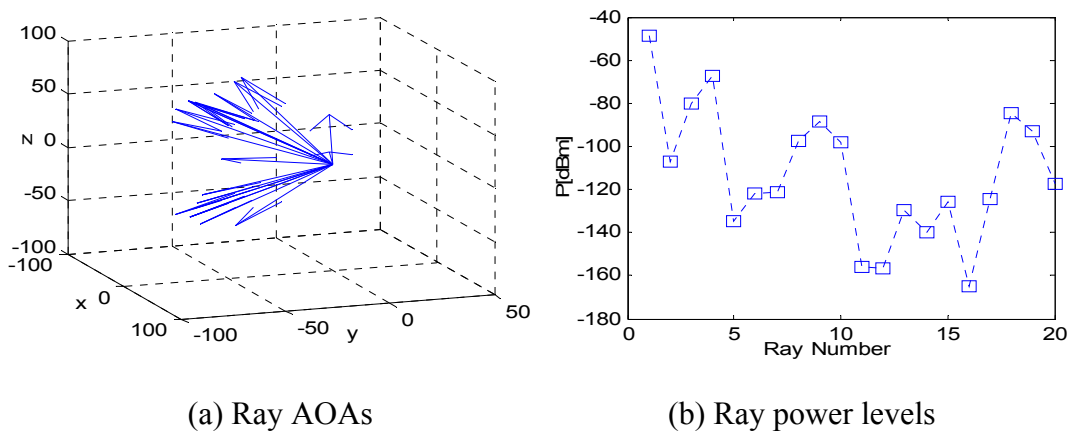
D.   Signal Rays Plots for Tx #4

(a) Ray AOAs

(b) Ray power levels

(c) Angle ϕ of rays

(d) Angle θ of rays

Figure 62.   Signal rays received by dipole receiver at location (145 m, 52 m, 1.5 m) when transmitting from Tx #4

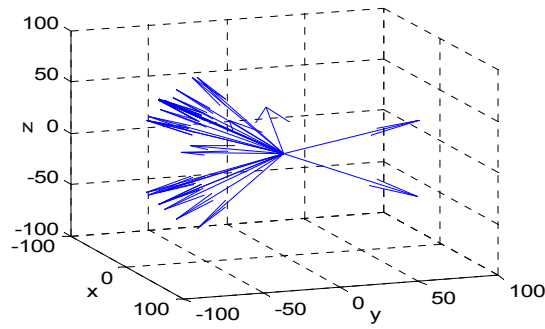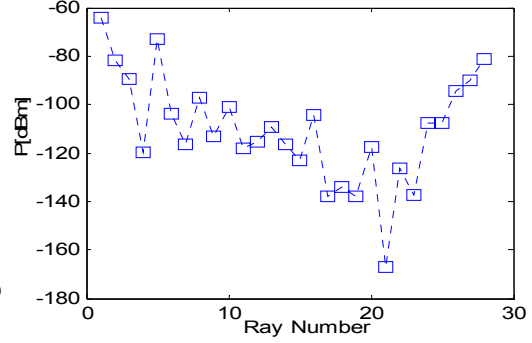(a) Ray AOAs

(b) Ray power levels

Figure 63.   Signal rays received by directional antenna at location (145 m, 52 m, 1.5 m) when transmitting from Tx #4
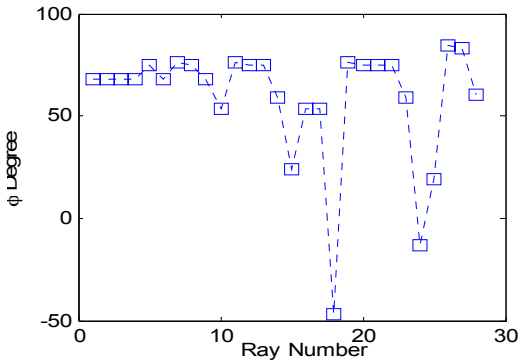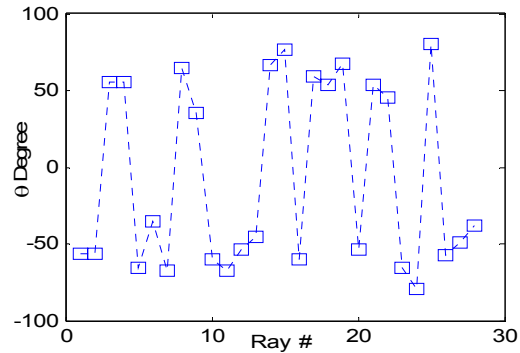
E.   Signal Rays Plots for Tx #5
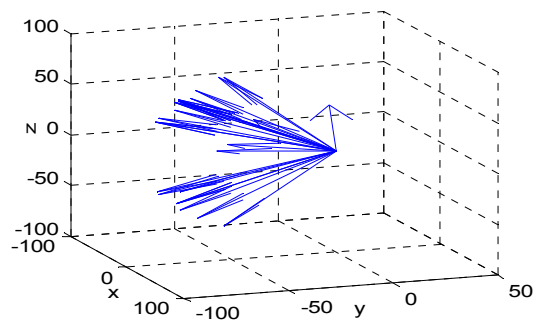

(a) Ray AOAs

(b) Ray power levels
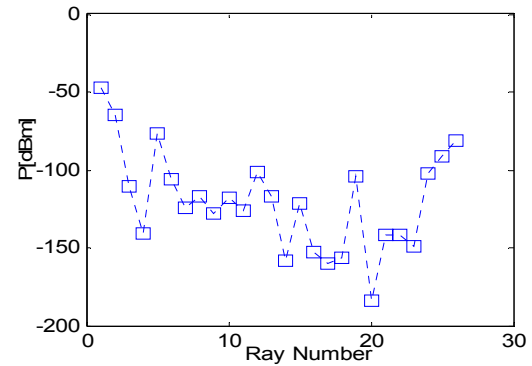

(c) Angle ϕ of rays

(d) Angle θ of rays

Figure 64.   Signal rays received by dipole receiver at location (145 m, 52 m, 1.5 m) when transmitting from Tx #5

(a) Ray AOAs

(b) Ray power levels

Figure 65.   Signal rays received by directional antenna at location (145 m, 52 m, 1.5 m) when transmitting from Tx #5

91

THIS PAGE INTENTIONALLY LEFT BLANK

LIST OF REFERENCES

[1] A. Vick, J. Stillion, D. Frelinger, J. Kvitky, B. Lambeth, J. Marquis, and M. Waxman, *Aerospace Operations in Urban Environments—Exploring New Concepts*, RAND, Santa Monica, CA, 2000.

[2] Lt. Col. D. Glade, USAF, "Unmanned Aerial Vehicles: Implications for Military Operations," Occasional Paper No. 16, Center for Strategy and Technology, Air War College, Air University, July 2000.

[3] D. W. Murphy and J. Cycon, "Applications for mini VTOL UAV for law enforcement", *Proceedings of SPIE Vol. 3577, Sensors, C3I, Information, and Training Technologies for Law Enforcement*, pp. 35-43, January 1999.

[4] www.globalsecurity.org, last accessed August 2004.

[5] www.fas.org, last accessed August 2004.

[6] S. J. A. Edwards, *Freeing Mercury's Wings—Improving Tactical Communications in Cities*, RAND, Santa Monica, CA, 2001.

[7] www.darpa.mil/ato/programs/acn.htm, last accessed August 2004.

[8] J. D. Parsons, *The Mobile Radio Propagation Channel*, John Wiley & Sons, Chichester, England, 2000.

[9] D. C. Jenn, Lecture notes for EC 3630, Radiowave Propagation, (unpublished), Spring 2004.

[10] J. Lebaric, Lecture notes for EC 4520, Smart Antennas, (unpublished), Spring 2004.

[11] S. R. Saunders, *Antennas and Propagation for Wireless Communication Systems*, John Wiley & Sons Ltd, Chichester, England, 1999.

[12] R. Janaswamy, *Radiowave Propagation and Smart Antennas for Wireless Communications*, Kluwer Academic Publishers, Norwell, MA, 2001.

[13] K. Siwiak, *Radiowave Propagation and Antennas for Personal Communications*, 2nd edition, Artech House, Norwell, MA, 1998.

[14] National Academy of Sciences, *The Evolution of Untethered Communications*, National Academy Press, Washington D.C., 1997.

[15] T. S. Rappaport, *Wireless Communications Principles and Practice,* 2nd edition, Prentice Hall PTR, Upper Saddle River, NJ, 2002.

[16] K. Dietze, "Analysis of a Two-Branch Maximal Ratio and Selection Diversity System with Unequal Branch Powers and Correlated Inputs for a Rayleigh Fading Channel", Master's Thesis, Virginia Polytechnic Institute and State University, March 2001.

[17] A. Naguib, V. Tarokh, N. Seshadri, and A. Calderbank, Presentation notes on Space-time Coding and Signal Processing for High Data Rate Wireless Communications, AT&T Labs-Research, Florham Park, NJ, 2004.

[18] S. Haykin and M. Moher, *Modern Wireless Communications*, Pearson Prentice Hall, Upper Saddle River, NJ, 2005.

[19] http://www.saic.com/products/software/urbana, last accessed September 2004.

[20] W. L. Lock, "Effects of Radio Wave Propagation in Urbanized Areas on UAV-GCS Command and Control", Master's Thesis, Naval Postgraduate School, Monterey, CA, December 2003.

[21] F. Pala, "Frequency and Polarization Diversity Simulations for Urban UAV Communication and Data Links", Master's Thesis, Naval Postgraduate School, Monterey, CA, September 2004.

INITIAL DISTRIBUTION LIST

1. Defense Technical Information Center
   Ft. Belvoir, Virginia

2. Dudley Knox Library
   Naval Postgraduate School
   Monterey, California

3. Chairman, Electrical & Computer Engineering Department
   Code EC
   Naval Postgraduate School
   Monterey, California

4. Professor David C. Jenn
   Code EC/Jn
   Naval Postgraduate School
   Monterey, California

5. Professor Jeffrey B. Knorr
   Code EC/Ko
   Naval Postgraduate School
   Monterey, California

6. Professor Jovan Lebaric
   Code EC/Lb
   Naval Postgraduate School
   Monterey, California

7. Professor Yeo Tat Soon
   Director, Temasek Defence Systems Institute
   National University of Singapore
   Singapore